Received: 7 May 2020 | Revised: 15 September 2020 | Accepted: 16 September 2020

DOI: 10.1111/ejn.14986

SPECIAL ISSUE ARTICLE

EJN European Journal of Neuroscience FENS WILEY

Phase-amplitude coupling profiles differ in frontal and auditory cortices of bats

Francisco García-Rosales[1] | **Luciana López-Jury**[1] | **Eugenia González-Palomares**[1] | **Yuranny Cabral-Calderín**[2] | **Manfred Kössl**[1] | **Julio C. Hechavarria**[1]

[1]Institut für Zellbiologie und Neurowissenschaft, Goethe-Universität, Frankfurt/M, Germany

[2]Research Group Neural and Environmental Rhythms, Max Planck Institute for Empirical Aesthetics, Frankfurt/M, Germany

Correspondence
Francisco García and Julio C. Hechavarria, Institut für Zellbiologie und Neurowissenschaft, Max-von-Laue-Str. 13, 60438 Frankfurt/Main, Germany.
Email: garciarosales@bio.uni-frankfurt.de; hechavarria@bio.uni-frankfurt.de

Funding information
Deutsche Forschungsgemeinschaft, Grant/Award Number: HE 7478/1-1

Abstract

Neural oscillations are at the core of important computations in the mammalian brain. Interactions between oscillatory activities in different frequency bands, such as delta (1–4 Hz), theta (4–8 Hz) or gamma (>30 Hz), are a powerful mechanism for binding fundamentally distinct spatiotemporal scales of neural processing. Phase-amplitude coupling (PAC) is one such plausible and well-described interaction, but much is yet to be uncovered regarding how PAC dynamics contribute to sensory representations. In particular, although PAC appears to have a major role in audition, the characteristics of coupling profiles in sensory and integration (i.e. frontal) cortical areas remain obscure. Here, we address this question by studying PAC dynamics in the frontal-auditory field (FAF; an auditory area in the bat frontal cortex) and the auditory cortex (AC) of the bat *Carollia perspicillata*. By means of simultaneous electrophysiological recordings in frontal and auditory cortices examining local-field potentials (LFPs), we show that the amplitude of gamma-band activity couples with the phase of low-frequency LFPs in both structures. Our results demonstrate that the coupling in FAF occurs most prominently in delta/high-gamma frequencies (1-4/75-100 Hz), whereas in the AC the coupling is strongest in the delta-theta/low-gamma (2-8/25-55 Hz) range. We argue that distinct PAC profiles may represent different mechanisms for neuronal processing in frontal and auditory cortices, and might complement oscillatory interactions for sensory processing in the frontal-auditory cortex network.

KEYWORDS

auditory cortex, cross-frequency coupling, delta oscillations, frontal cortex, gamma oscillations, local-field potentials, phase-amplitude coupling, theta oscillations

Abbreviations: (z)MI, (z-scored) modulation index; AC, auditory cortex; FAF, frontal-auditory field; FDR, false discovery rate; LFP, local-field potential; PAC, phase amplitude coupling; PAC_{AC}, PACFAF: PAC in AC, PAC in FAF, respectively.

Edited by Prof. Antoine Adamantidis

1 | INTRODUCTION

There is increasing evidence supporting the role of oscillatory activity as instrument of neural computations in the mammalian brain. Oscillations in low- and high-frequencies, particularly in the delta-to-alpha (1–12 Hz) and gamma (>30 Hz) ranges, are deemed essential for numerous tasks, including sensory processing and selectivity (Bosman et al., 2012; Obleser & Kayser, 2019; Schroeder & Lakatos, 2009), the implementation of attentional mechanisms (Lakatos et al., 2013; Magazzini & Singh, 2018), cognitive control (Cho et al., 2006; Helfrich & Knight, 2016), learning and memory (Benchenane et al., 2010; Wang et al., 2018) or inter-areal connectivity by means of communication-through-coherence (Fries, 2015). High- and low-frequency oscillations represent the activity of local and global neuronal ensembles, respectively, occurring at different timescales determined by the oscillatory frequencies (Canolty & Knight, 2010). The question of how different spatiotemporal scales are integrated in the brain, and therefore the relationship between co-existing low- and high-frequency activities, has gained attention in recent years.

Cross-frequency coupling is a plausible mechanism that could allow for the binding of low- and high-frequency oscillations and their respective spatiotemporal dynamics (Canolty & Knight, 2010; Hyafil et al., 2015; Tort et al., 2010). A specific form of cross-frequency coupling, namely phase-amplitude coupling (PAC), has been related to numerous brain functions. PAC is the phenomenon whereby the phase of a low-frequency oscillation couples with the amplitude of a high-frequency one. This type of interaction between distinct frequency bands is well-established in regions such as the hippocampus (Lisman & Jensen, 2013), the frontal cortex (Helfrich & Knight, 2016) and cortical sensory areas (Esghaei et al., 2015; O'Connell et al., 2015; Sotero et al., 2015; Spaak et al., 2012; Xiao et al., 2019). PAC in these regions has been associated with working memory (Axmacher et al., 2010; Daume et al., 2017), learning (Tort et al., 2009), behavioural coordination (Amemiya & Redish, 2018), and the organization of inter-areal communication and information binding (Colgin et al., 2009; Daume et al., 2017). High-order sensory processing may also capitalize on PAC, the latter providing a mechanistic substrate for the parsing of continuous stimuli by accommodating local network activity in the gamma range into slower, behaviourally relevant timescales represented by the low-frequency activity (Giraud & Poeppel, 2012; Hyafil, et al., 2015). Indeed, theta-gamma coupling in the auditory cortex (AC) of humans has been suggested as vital component of speech processing (Giraud & Poeppel, 2012; Gross et al., 2013; Hyafil et al., 2015; Morillon et al., 2012), while it has been shown that similar PAC profiles in the primate AC mediate acoustic sequence learning (Kikuchi et al., 2017).

At present, little is known about PAC dynamics in auditory regions of animal models beyond primates. However, tackling such question can provide valuable insights into the nature of evolutionarily preserved circuits across species. In both primates and non-primates there exist structures in the frontal cortex that are strongly responsive to acoustic stimuli (Eiermann & Esser, 2000; Kobler et al., 1987; Medalla & Barbas, 2014; Plakke & Romanski, 2014). Within these structures, the relationship between the phase of low frequency oscillations and the amplitude of high frequency rhythms remains largely unexplored. The current study aims to bridge this gap by means of electrophysiological recordings of local-field potentials (LFPs) from the AC and a region of the short-tailed bat's (*Carollia perspicillata*) frontal cortex, specialized for audition: the frontal-auditory field (FAF; (Eiermann & Esser, 2000; Kobler et al., 1987)). In previous work we showed robust oscillatory responses to acoustic stimulation in *C. perspicillata's* FAF and AC (García-Rosales et al., 2020; Hechavarria et al., 2016b), and that in the latter structure low-frequency LFPs could be crucial for the neuronal coding of naturalistic sequences (García-Rosales et al., 2018a; García-Rosales et al., 2018b). Furthermore, we observed functional coupling in the FAF-AC circuit by means of delta- (without auditory input) and gamma-band LFPs (García-Rosales et al., 2020). The above supports the roles of cortical oscillations for auditory computations in fronto-temporal networks in mammals.

In this paper, we characterized PAC profiles in FAF and AC during spontaneous activity and sound processing. We found that high-frequency amplitude was coupled to the phase of low-frequency rhythms in frontal and auditory cortices. However, the specific frequencies at which this occurred differed across structures, both with and without acoustic stimulation. Delta/high-gamma PAC was typical in FAF, whereas delta-theta/low-gamma coupling occurred most prominently in the AC. We argue that distinct PAC profiles in FAF and AC could represent distinct mechanisms of neural processing at the level of sensory and association areas.

2 | MATERIALS AND METHODS

2.1 | Animal preparation and surgical procedures

The study was conducted using five awake *Carollia perspicillata* bats (all males). All experimental procedures were in compliance with European regulations on animal experimentation, and approved by the Regierungspräsidium Darmstad (experimental permit

#FU-1126). Animals were obtained from a colony at the Goethe-University in Frankfurt. Bats used for experiments were isolated from the main colony.

Surgical and experimental procedures are described in detail in a previous study (García-Rosales et al., 2020), which addressed the functional connectivity between the frontal-auditory field and the auditory cortex of this bat species. The current study capitalizes on the same dataset from (García-Rosales et al., 2020) in order to investigate the dynamics of phase-amplitude coupling in the frontal and auditory cortices of *C. perspicillata*. In brief, for surgery, animals were anaesthetized with a mixture of ketamine-xylazine (ketamine: 10 $mg*kg^{-1}$, Ketavet, Pfizer; xylazine: 38 $mg*kg^{-1}$, Rompun, Bayer), and their auditory and frontal cortices exposed by means of a small craniotomy (ca. 1 mm^2) performed with a scalpel blade. The anatomical location of the two regions of interest was assessed by means of well-described landmarks in both frontal and auditory areas (Eiermann & Esser, 2000; Esser & Eiermann, 1999). After surgery, animals were allowed to recover for at least two days before undergoing experiments. Recordings lasted no more than 4 hr per session, and each bat was allowed to recover between sessions for at least a full day. Water was given to the bat at periods of ~1–1.5 hr, and experiments for the day were halted if the animal showed any sign of discomfort.

2.2 | Electrophysiological recordings

Electrophysiological data were acquired inside a sound-proof and electrically isolated chamber, where bats were placed on a custom-made holder which was kept at a constant temperature of 30°C with a heating blanket (Harvard, Homeothermic blanket control unit). A speaker (NeoCD 1.0 Ribbon Tweeter; Fountek Electronics), used for free-field stimulation, was positioned 12 cm away from the bat's right ear, contralateral to the hemisphere on which recordings were made. Speaker calibration was done with a ¼-inch microphone (Brüel & Kjær, model 4,135, Denmark), connected to a custom-made amplifier.

Recordings were made from the FAF and AC of the left hemisphere. As described in previous studies (García-Rosales et al., 2020; Garcia-Rosales et al., 2019), a NeuroNexus laminar probe (Model A1x16, impedance: 0.5–3 MΩ; 50 μm channel spacing) was carefully inserted perpendicularly into the AC until the uppermost channel was barely visible at the cortical surface. Therefore, the probe's channels spanned depths from 0–750 μm, covering the extent of an auditory cortical column in *C. perspicillata's* brain (see (Garcia-Rosales et al., 2019)). Recordings in the FAF were performed, simultaneously to those in the AC, with a single carbon electrode (Carbostar-1, Kation scientific; Impedance at 1 kHz: 0.4–1.2 MΩ), at cortical depths of ~300–450 μm (313 +-56 μm; mean +- std).

Both the probe in the AC and the carbon electrode in the FAF were connected each to their own micropreamplifier (MPA 16, Multichannel Systems MCS GmbH, Reutlingen, Germany), which were in turn connected to an integrated amplifier and analog-to-digital converter with 32-channel capacity (Multi Channel Systems MCS GmbH, model ME32 System, Germany). The sampling frequency of the recordings was 20 kHz, and the precision was 16 bits. Data were visualized online and stored in a computer using the MC_Rack_Software (Multi Channel Systems MCS GmbH, Reutlingen, Germany; version 4.6.2).

2.3 | Acoustic stimulation

Acoustic stimulation was controlled with a custom-written Matlab (version 7.9.0.529 (R2009b), MathWorks) software. Sounds consisted of a natural distress sequence, which is representative of this bat species' distress repertoire (for recording details and sequence characteristics, see (García-Rosales, et al., 2018; Hechavarria et al., 2016a)), as well as two artificially constructed syllabic trains. One of these trains consisted of a single distress syllable (also representative of *C. perspicillata's* distress repertoire) repeated isochronously at a rate of 5.28 Hz for a period of 2 s. The second syllabic train consisted of the same syllable repeated with an average rate of 70 Hz, in a Poisson-like manner, with a duration of 4 s. The rate of the 5.28 Hz and the Poisson train (70 Hz) stimuli were chosen to match the slow and fast periodicities typically present in distress sequences of *C. perspicillata*, which range between 4–12 and >50 Hz, corresponding to the bout and syllabic rhythms (respectively) of the calls. The Poisson train further allows to probe neural dynamics in the presence of fastly repeated distress syllables without a low-frequency rhythmicity that might entrain delta-theta oscillations to the structure of the stimulus. The spectrogram and oscillogram of the sequences, as well as the spectrogram of the syllable used to construct the artificial trains, are depicted in Figure 1.

Auditory stimuli were digital-to-analog converted using a sound card (M2Tech Hi-face DAC, 384 kHz, 32 bit; sampling frequency used: 192 kHz due to technical reasons), amplified (Rotel power amplifier, model RB-1050), and fed to the speaker inside the chamber (description above). Before presentation, sounds were low-pass filtered (80 kHz) and down-sampled to 192 kHz to avoid aliasing artefacts. Stimuli were presented 50 times each, in a pseudorandom order, with an inter-stimulus interval of 1 s. A period of 300 ms and another of 500 ms of silence was padded at the beginning and the end of each sequence, respectively. Before presenting the stimulus battery, 180 s of spontaneous activity were recorded per penetration.

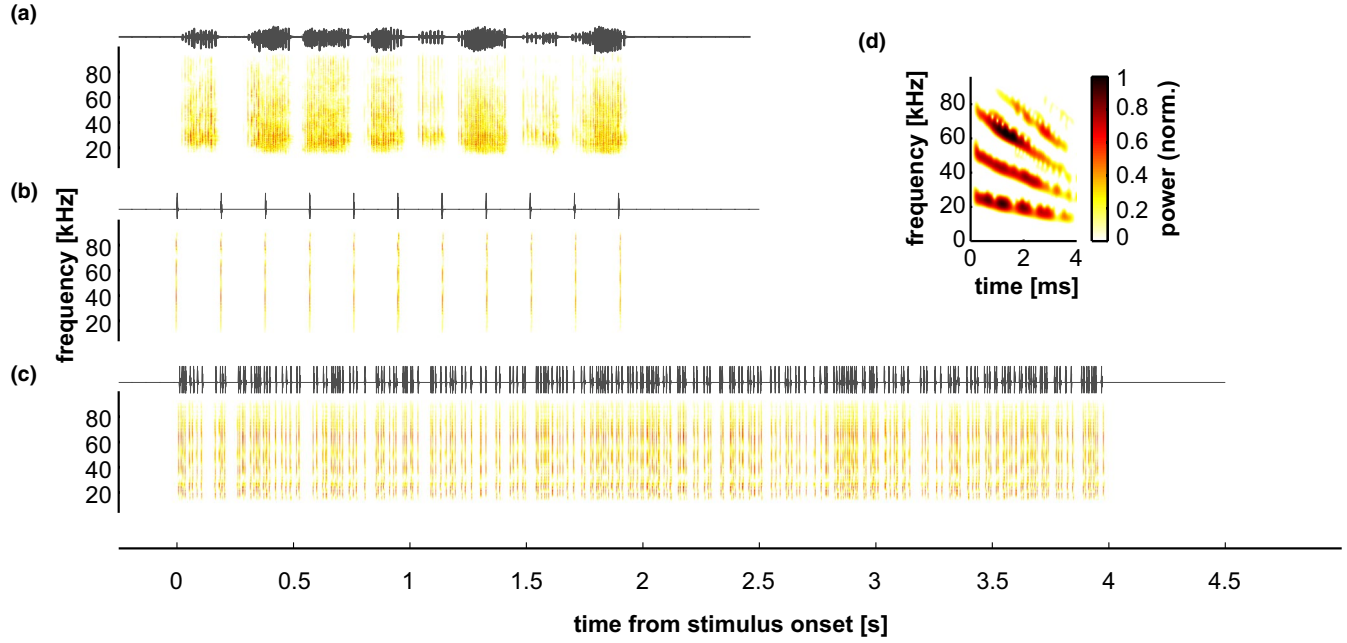

FIGURE 1 Auditory stimuli. Oscillograms (top) and spectrograms (bottom; normalized amplitude and power) of the sounds used for auditory stimulation. These comprised a natural call (a), a syllable train with a repetition rate of 5.28 Hz (b), and a syllable train with a Poisson temporal structure (c). Panel D shows the spectrotemporal design of the natural distress syllable used to construct the trains in B and C

2.4 | Separation of local-field potentials

Data analyses were performed offline using custom-written Matlab scripts (version 8.6.0.267246 (R2015b)). The raw signal from each channel (either FAF or the 16 channels in the AC) was band-pass filtered between 0.1 and 300 Hz (4th order Butterworth filter, in the forward and backward directions; Matlab function *filtfilt*) in order to obtain local-field potentials. For computational reasons, LFPs were down-sampled to 1 kHz and stored in order to be used in subsequent analyses.

2.5 | Phase-amplitude coupling

Phase-amplitude coupling was calculated for each stimulus and spontaneous activity per penetration, based on previously published methodology (Kikuchi et al., 2017). For low frequencies, which provided the phase reference, LPFs were filtered (4th order bandpass Butterworth filter; Matlab function *filtfilt*) in the following bands: 1–3, 3–5, 5–7, … , and 13–15 Hz, thus having centre frequencies of 2, 4, 6, … 14 Hz, with 2 Hz bandwidth. For higher frequencies, providing the amplitude, LFPs were filtered in bands of 25–35, 30–40, 35–45, …, and 120–130 Hz, therefore having centre frequencies of 30, 35, 40, 45, … , 125 Hz, with 10 Hz bandwidth. After filtering and applying the Hilbert transform on the signals (see below), only the time window between stimulus onset and offset was considered for analysis in a trial.

For analysing sound-related LFP responses, the instantaneous phase [ϕ (t)] and amplitude [$A(t)$] of the signal were extracted from low and high frequency filtered LFPs, respectively, by means of a Hilbert transform. To reduce the effect of the stimulus-evoked responses, which could affect PAC values and bias true interactions (Aru et al., 2015), before filtering and determining $\phi(t)$ and $A(t)$ per trial, the average of across trials for the current stimulus and penetration ($n = 50$ trials) was subtracted from the individual response of each trial. The former has the consequence of reducing the effect of time-locked responses in the LFPs for PAC calculations (Kikuchi et al., 2017). Additionally, to minimize the effect of phase non-uniformities (clustering) in the LFPs caused by non-oscillatory periodicities in the field potentials, which could also bias PAC estimates (van Driel et al., 2015), the mean vector of the phase angles was linearly subtracted from the instantaneous phase time series as follows:

$$\phi'(t) = e^{i\phi(t)} - \frac{1}{n}\sum e^{i\phi(t)}, \quad (1)$$

where $\phi'(t)$ denotes the corrected phase (i.e. after phase-cluster de-biasing) at time t, and n represents the number of time points in the series. With $\phi'(t)$ and $A(t)$, a composite time series $z(t) = A(t) \times \phi'(t)$ was constructed. From $z(t)$ the modulation index (MI) was quantified as:

$$MI = \left| \frac{1}{n}\sum z(t) \right| \quad (2)$$

PAC suffers from a number of caveats that depend on the way it is calculated, and on the temporal structure and statistical properties of the LFPs (Aru et al., 2015). As mentioned above, we took measures to minimize possible confounding effects by subtracting the trial-average from each individual trial in response to a stimulus, and by addressing the bias introduced by phase-clustering. In addition to those steps, we calculated a surrogate MI (MI_{surr}) by matching the phase series $\phi'(t)$ of a given trial k with the amplitude $A(t)$ of another trial m (see Figure 3a and (Aru et al., 2015; Kikuchi et al., 2017)). The trial-shuffling approach further allows to control more stringently for the effect of evoked responses in the LFPs, given that the average evoked-related amplitude and phase responses are unaltered and therefore contribute to the PAC in a similar way as the non-shuffled response. On the other hand, any contribution to the PAC that was trial-by-trial variable would be abolished with the trial-shuffling procedure. Amplitude and phase were paired at random across trials a large number of times (250 permutations), and a modulation index calculated for each iteration. This surrogate method yields a null distribution that accounts for PAC attributable to evoked responses, while allowing to examine trial-specific coupling (Kikuchi et al., 2017). Modulation indexes obtained with the non-surrogate data ("direct analysis" in Figure 3) were z-normalized to the null distribution obtained by the surrogate approach (zMI). If no effect of PAC exists in the data, zMI values would hover around 0, whereas coupling effects would yield zMIs significantly higher than 0. To assess the former, we used a z-score of 2.5 (i.e. 2.5 standard deviations from the null) as threshold per penetration (see Figure S1).

The quantification of spontaneous PAC was similar to that of the stimulus-related PAC. LFP chunks ($n = 50$; same as the number of trials used during stimulation) were selected randomly from the 180 s window of a given penetration, with a length of 1.964 s (the same length as the natural call used for stimulation), and without overlap. Before chunking, the 180 s window was filtered and Hilbert-transformed for obtaining phase and amplitude series, in order to avoid edge artefacts in the filtered and transformed LFP segments. Because there was no temporal frame of reference, chunk averaging was not performed for subtraction. Chunks were treated as stimulation trials (see above), and PAC analyses together with surrogate calculations were applied in likeness to those performed with stimulus-driven responses.

To test for a population trend of positive PAC, we evaluated, per phase-amplitude frequency pair, whether zMIs for the population were significantly higher than 0 (FDR-corrected, tailed Wilcoxon signed rank test, significance after $p_{corr} < .05$). This is indicated as grey lines in Figures 4 and 5.

Differences between the PAC in FAF (PAC_{FAF}) and AC (PAC_{AC}) were obtained by subtracting the PAC maps calculated in frontal and auditory cortices, the latter considering five representative depths of 50, 300, 450, 600, 750 μm. Significant differences between channels in FAF and AC were determined by means of FDR-corrected Wilcoxon signed rank tests, and significance was considered when $p_{corr} < .05$. Beyond significance testing, we evaluated the effect size of the difference between PAC_{FAF} and PAC_{AC} as follows (Fritz et al., 2012):

$$r = \frac{W}{\sqrt{N}} \tag{4}$$

where r is the effect size, W is the test statistic of the Wilcoxon signed rank test, and N is the sample size ($N = 50$ penetrations during acoustic processing, and $N = 49$ during spontaneous activity). Note that the spontaneous activity of one of the penetrations could not be evaluated due to technical reasons. According to (Fritz et al., 2012) values of $r < 0.3$ were considered negligible effects, whereas values of $0.3 \leq r \leq 0.5$ were considered medium, and values of $r > 0.5$ were considered large effects. Only large effects are depicted in the figures as contour lines. Positive large effects (red contour lines) indicate $PAC_{FAF} > PAC_{AC}$, whereas negative large effects (purple contour lines) indicate the opposite.

To evaluate whether the PAC patterns were independent of the described methodology for estimating the coupling, we also computed PAC by means of the procedure proposed by Tort and colleagues (Tort et al., 2010). Here, data were treated in the same manner as above (i.e. same frequency bands for phase and amplitude, filter settings, and surrogate analyses), except for the subtraction of the average vector length (as per (van Driel et al., 2015)) from the phase time series, which was not performed. PAC profiles were very similar using either method, as seen from exemplary population coupling profiles, obtained using Tort et al.'s procedure, in Figure S2.

3 | RESULTS

3.1 | Neural responses in the FAF and AC of *C. perspicillata*

Electrophysiological experiments were performed on five adult male *Carollia perspicillata* bats. We recorded a total of 50 penetrations pairs, each pair comprised of simultaneously recorded neural activity in the FAF and AC. In the FAF, a single carbon electrode was inserted, and recordings were made at depths ranging from 300–450 μm. In the AC, a 16-channel probe was used, allowing to record from cortical depths spanning 0–750 μm at once. Both spontaneous (i.e. without acoustic stimulation) and auditory-driven neural activities were analysed. Auditory stimuli consisted of a natural call (henceforth, "nat" stimulus) representative of this species distress repertoire (Figure 1a; see (Hechavarria et al., 2016a)), as well as two artificially constructed syllabic trains (see Methods and

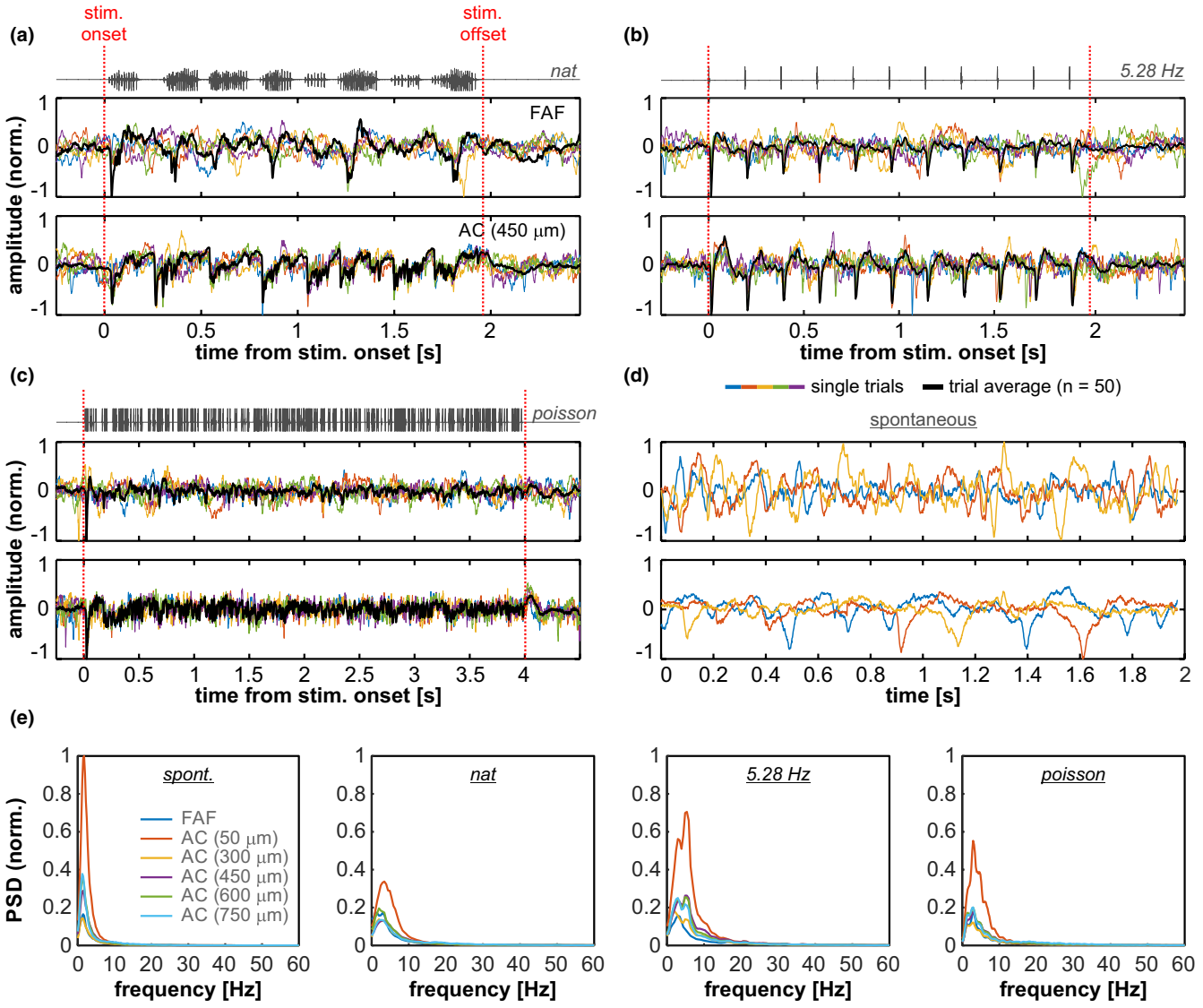

FIGURE 2 Representative LFP recordings during auditory processing and spontaneous activity. (a) LFP traces from the FAF (top) and the AC at a depth of 450 µm (bottom), in response to the natural call (stimulus' oscillogram shown on top of the subpanels). Coloured lines correspond to five single-trial recordings (out of a total of 50 trials) from a representative penetration. The thick black line depicts the trial average. Vertical red dashed lines mark the onset and offset of the stimulus. (b) Same as in A, but LFPs were recorded in response to the 5.28 Hz syllabic train. (c) Same as in A and B, but responses correspond to the Poisson train. (d) Three representative chunks of spontaneously recorded LFP signals of the same penetration shown in A-C. Note that a trial average is lacking as chunks do not share a reference time point (e.g. stimulus onset). In all panels, single-trial LFP traces from FAF and AC with the same colour were recorded simultaneously. (e) Normalized population-averaged power spectral density (PSD) of the LFP signals recorded during spontaneous activity, and during acoustic stimulation. Within each panel (left to right: spontaneous activity, stimulation with the natural call, stimulation with the 5.28 Hz train, and stimulation with the Poisson train) data are shown from the FAF and five representative depths in the AC (50, 300, 450, 600 and 750 µm). The trial average was subtracted from single trials related to sound presentation before the power spectrum was calculated (see Methods). During spontaneous activity $n = 49$ penetrations were considered; during acoustic stimulation data from $n = 50$ penetrations are shown

(García-Rosales et al., 2020)). The first of these trains had an isochronous structure by which a natural syllable was repeated with a rate of 5.28 Hz (Figure 1b). In the second train, the same syllable was repeated in a Poisson-like manner (i.e. non-periodically) with an average rate of 70 Hz (Figure 1c). The 5.28 and 70 Hz rates were selected to resemble the slow and fast temporal structures of distress vocalizations of *C. perspicillata*, which possess bout- and syllabic- rhythms in the range of ~4–12 Hz and >50 Hz, respectively (Hechavarria et al., 2016a). The natural syllable used to construct these trains was also typical for distress syllables in this bat species (Hechavarria et al., 2016a); its time-frequency representation is shown in Figure 1d.

Local-field potentials were analysed for each penetration pair in FAF and AC. We observed robust auditory responses in the LFPs of both structures, as illustrated for a representative penetration pair in Figure 2a-c, where single trial responses

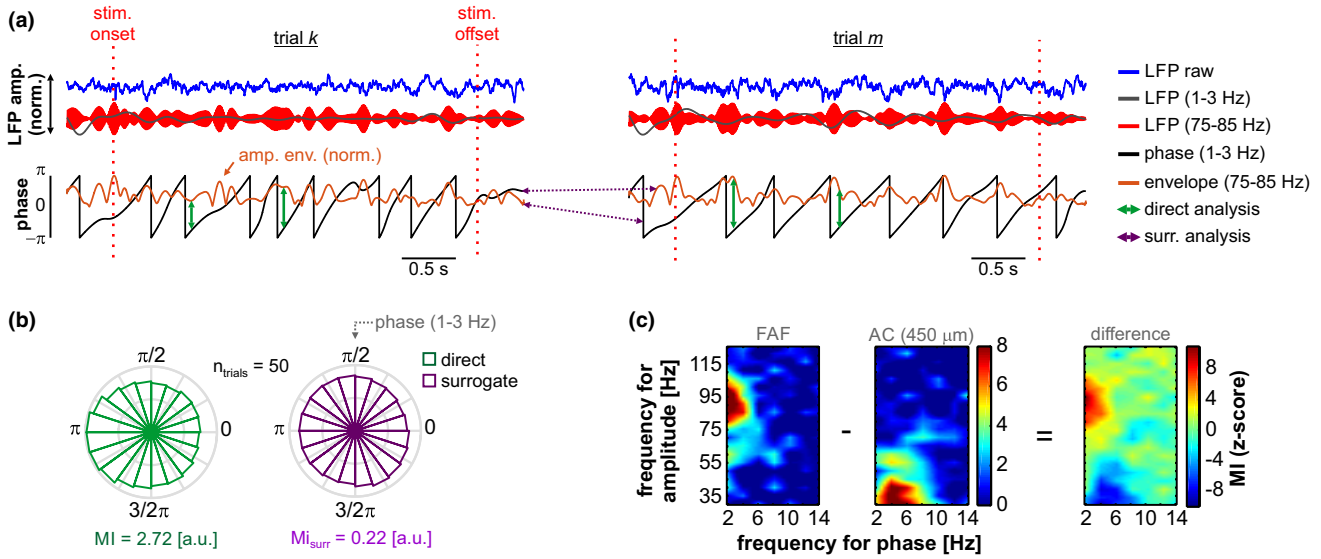

FIGURE 3 Phase-amplitude coupling analyses in representative recordings. (a) Single trial LFPs (2 exemplary trials *k* and *m*, blue traces), recorded from the FAF, in response to the Poisson syllabic train. Stimulus onset and offset are marked with red vertical dashed lines; the window between onset and offset was used for PAC analyses across stimuli (here, 4 s length). Delta- (1–3 Hz) and gamma-band (75–85 Hz) filtered LFPs are depicted in grey and red, respectively. Note that 1–3 Hz (within the delta range) is one of the bands in which LFPs were filtered for analyses, chosen here for illustrative purposes (see Methods). Below, the phase of the delta LFPs (black) and the amplitude envelope of gamma (orange) are shown. In a direct PAC analysis, phase and amplitude were matched within trials (represented with green arrows in the figure). However, during surrogate analyses, amplitude and phase were matched between trials at random (trial shuffling; see Methods). The latter is depicted as purple arrows across trials *k* and *m*. (b) Circular distribution depicting the relationship between gamma-band amplitude and delta-band phase. With the direct analysis, the phase-amplitude relationship was visibly non-circularly uniform (green), yielding a modulation index (MI) of 2.72. In an instance of the surrogate analysis (purple), shown for illustrative purposes, the phase-amplitude relationship was distributed rather uniformly, yielding a MI of 0.22. (c) Phase-amplitude coupling (PAC) maps calculated from LFPs corresponding to the same penetration shown in A and B, also in response to the Poisson train. The PAC is shown for the FAF and the AC at a depth of 450 µm. To evaluate differences in the PAC across structures, maps from FAF and AC were subtracted in further analyses (here shown as "difference")

to each stimulus (coloured traces) are shown together with the trial-average LFPs for the penetration (black). In the panels of Figure 2, data are shown from the FAF and the AC, the latter at a depth of 450 µm (top and bottom subpanels, respectively). Single trials in FAF and AC depicted with the same colour were recorded simultaneously. Figure 2d illustrates LFP chunks (see Methods) corresponding to spontaneous activity. Note that no trial-average is shown because there are no temporal references for inter-chunk averaging, such as the onset of a stimulus. Figure 2e depicts the power spectral densities (PSD; grand average across penetrations) from field potentials recorded in FAF and AC during spontaneous activity and acoustic processing, the latter region at representative depths of 50, 300, 450, 600 and 750 µm. Prominent low-frequency activity is evident from the peak of the power spectra across conditions and structures.

3.2 | Phase amplitude-coupling in FAF and AC

We evaluated phase-amplitude coupling between low and high frequencies in FAF and AC using a procedure inspired by a previous study (Kikuchi et al., 2017). LFPs for phase were filtered (4th order bandpass Butterworth) in frequency bands with centres at 2, 4, 6, …, 14 Hz, and 2 Hz bandwidth. LFPs for amplitude were filtered (same filter as before) in frequency bands centred at 30, 35, 40, …, 125 Hz, with 10 Hz bandwidth. Figure 3a illustrates two single-trial recordings from the FAF in response to the Poisson train. Delta- (1–3 Hz) and gamma-band (75–85 Hz; bands chosen for illustrative purposes) LFPs are shown in grey and red, respectively. The instantaneous phase and amplitude of delta and gamma LFP signals are also shown in black and orange, respectively. Instantaneous phase and amplitude were extracted after Hilbert-transforming the filtered LFPs. To correct for possible biases due to phase non-uniformity in the signals (Aru et al., 2015; van Driel et al., 2015), the mean phase vector was linearly subtracted from the instantaneous phase series. PAC in FAF and AC (PAC_{FAF} and PAC_{AC}, respectively) were quantified by z-normalizing a modulation index (MI; z-normalized index: zMI) to a surrogate distribution where effects of evoked-related responses across trials were tackled (Figure 3a,b; see Methods for details). Based on the zMIs we obtained PAC profiles for each channel and penetration.

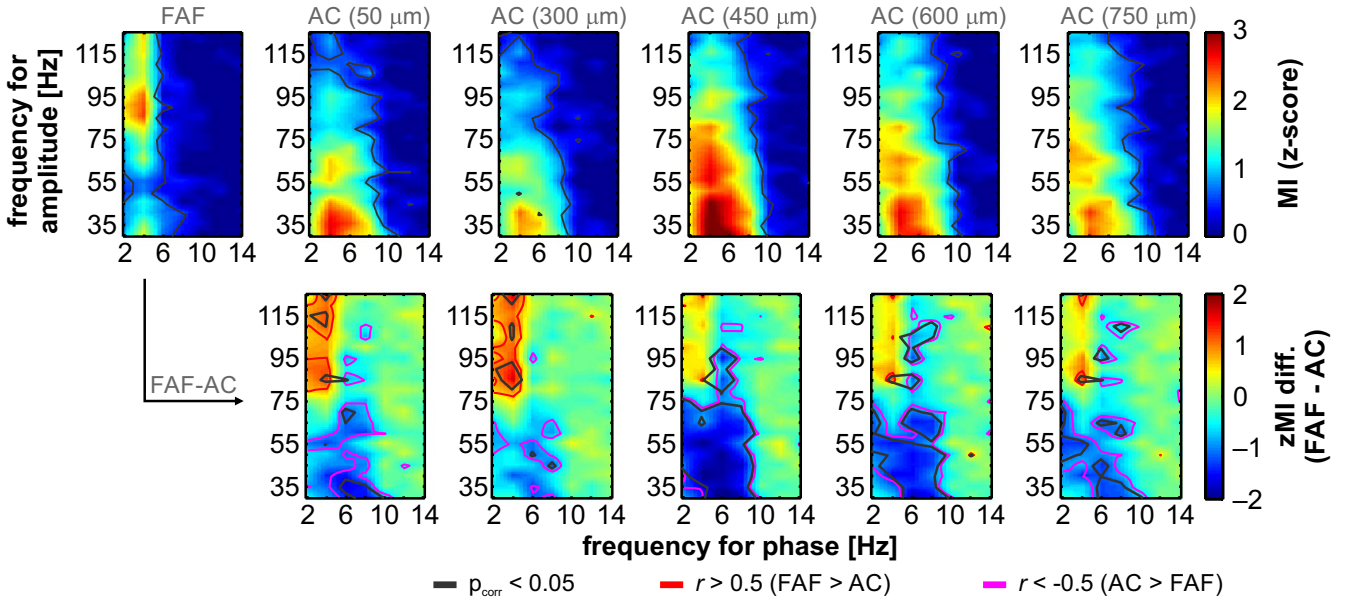

FIGURE 4 Spontaneous PAC in FAF and AC. (*Top*) Population-averaged PAC maps calculated from spontaneously recorded LFPs in the FAF and AC (here shown at depths of 50, 300, 450, 600 and 750 μm). Regions within grey contour lines correspond to those for which z-normalized MIs were significantly above 0 across penetrations ($n = 49$; FDR-corrected Wilcoxon signed rank test, $p_{corr} < .05$). (*Bottom*) PAC-difference maps between FAF and AC at the same depths from A. Red contour lines delimit regions where PAC in FAF (PAC_{FAF}) was higher than the PAC in AC (PAC_{AC}), with a large effect size ($r > 0.5$). Purple contour lines delimit regions where the opposite occurred (i.e. $PAC_{AC} > PAC_{FAF}$). Grey contour lines mark PAC regions where the differences were significant, after an FDR-corrected Wilcoxon signed rank test (comparing PAC_{FAF} vs PAC_{AC}), at an alpha of 0.05

Across penetrations, and as is readily visible in Figure 3c, the PAC in the FAF typically peaked in the delta/high-gamma range of the PAC maps (δ/γ_{high}; i.e. frequency for phase: ~1–4 Hz, frequency for amplitude: ~70–100 Hz). On the other hand, the PAC in the AC was strongest in channels located in input layers (depths of 300–550 μm), and the values of zMI typically peaked in the delta-theta/low-gamma range of the maps (δ–θ/γ_{low}; frequency for phase: ~2–8 Hz, frequency for amplitude: ~25–55 Hz). This trend occurred even without acoustic stimulation, as depicted in Figure 4 (*top*), where population-level spontaneous PAC profiles are shown for the FAF and the AC, the latter at representative depths of 50, 300, 450, 600 and 750 μm. We observed that zMIs across the population were significantly higher than 0 in both FAF and AC (regions delimited by grey contour lines; FDR-corrected tailed Wilcoxon signed rank tests, $p_{corr} < .05$), and that significant zMIs within single penetrations (i.e. zMIs > 2.5; see Methods) occurred in ~40% of the cases (out of $n = 49$ penetrations; 1 penetration could not be examined during spontaneous activity) in FAF, mostly located in the δ/γ_{high} range of the PAC space, and in ~40%–50% of the cases in the AC (most strongly for depths of 450 μm), mostly in the δ–θ/γ_{low} range of the PAC space. The quantification of the percentage of significant PAC across the population is shown in Figure S1.

Regarding the regions in which the coupling peaked, there was a clear distinction between the PAC_{FAF} and the PAC_{AC}. The difference was evaluated by subtracting the PAC values calculated in the AC from those calculated in the FAF, as illustrated in Figure 3c. By systematically doing so across penetrations in our dataset, consistent dissimilarities between PAC_{FAF} and PAC_{AC} profiles became evident during spontaneous activity (Figure 4, bottom). The spontaneous PAC_{FAF} appeared to be higher than the PAC_{AC} in the δ/γ_{high} range, particularly for superficial layers (0–300 μm) of the AC. In this case, although significance did not survive multiple comparisons consistently (FDR-corrected Wilcoxon signed rank tests, corrected threshold at $p_{corr} = .05$; grey contour lines), effect size estimations (r; see Methods) yielded large effects ($r > 0.5$, after (Fritz et al., 2012)) in the δ/γ_{high} range (red contour lines in Figure 4, bottom). Large differences did not occur in this PAC range when considering middle or deep layers of the AC, which could be attributable to the extent of relatively high PAC values to gamma frequencies up to ~80 Hz (see Figure 4, top). In addition, spontaneous PAC_{AC} values were higher than PAC_{FAF} ones in the δ–θ/γ_{low} range, reaching significance at AC depths > 450 μm (grey contour lines in Figure 4, bottom; FDR-corrected Wilcoxon signed rank tests, $p_{corr} < .05$). Still, even in cases where significance did not survive corrections for multiple comparisons (i.e. depths < 300 μm), we observed large effect sizes indicating that there was a consistent trend of PAC_{AC} being higher than PAC_{FAF} in δ–θ/γ_{low} frequencies ($r > 0.5$, purple contour lines in Figure 4, bottom).

3.3 | Population-level PAC in FAF and AC during acoustic processing

The PAC patterns in frontal and auditory cortices remained almost qualitatively unaltered during acoustic stimulation. Figure 5 depicts PAC maps from AC and FAF, in a similar arrangement to Figure 4, but using stimulus-driven LFPs recorded in response to the natural call, and to the 5.28 Hz and Poisson syllabic trains (Figure 5a-c, respectively). In each panel of Figure 5, averaged PAC profiles from the FAF and AC are depicted on the top row (AC at depths of 50, 300, 450, 600 and 750 μm), while the differences between structures are shown in the bottom row. Similar to what occurs during spontaneous activity, population-level PAC_{FAF} was strongest in the δ/γ_{high} range, while the PAC_{AC} peaked in the δ–θ/γ_{low} range (more markedly at depths of 450 μm). The former was true independently of the stimulus used. Indeed, we observed that zMIs in FAF and AC were significantly above zero across penetrations (Figure 5a-c, top row in panels; FDR-corrected tailed Wilcoxon signed rank tests, $p_{corr} < .05$), and that the PAC regions where this happened were predominantly those of δ/γ_{high} and δ–θ/γ_{low} in FAF and AC, respectively. Individually within penetrations and across stimuli, we observed significant zMIs (>2.5; see Methods) in the FAF occurring in δ/γ_{high} frequencies for ~40%–56% of the penetrations. Significant zMIs were observed in the AC, at 450 μm, for ~20%–25% of the penetrations (see also Figure S1). The decline in the percentage of significant zMIs during acoustic stimulation in the AC can be explained by the stringency of the surrogate analyses used, and by the efforts made to minimize the effect of stimulus-evoked responses in PAC calculations (see Methods). Note that the surrogate analyses, in conjunction with the subtraction of the mean across trials, may affect z-scored PAC values that are not only explained by broadband evoked responses, but that are however temporally locked to the stimuli. These did not strongly affect the data from the FAF. The increase of percentage of significant penetrations within FAF in the δ/γ_{high} range indicates a modulation of PAC strength by acoustic stimulation.

Differences between PAC_{FAF} and PAC_{AC} during acoustic processing occurred predominantly in the δ/γ_{high} and δ–θ/γ_{low} ranges (Figure 5a-c, bottom row in panels). The PAC_{FAF} was significantly stronger than the PAC_{AC} in δ/γ_{high} frequencies at all recording depths of the AC (FDR-corrected Wilcoxon signed rank tests, $p_{corr} < .05$), with large effect sizes ($r > 0.5$; red contour lines in Figure 5a-c, bottom) for all stimuli. Conversely, the PAC_{AC} appeared stronger than the PAC_{FAF} in δ–θ/γ_{low} frequencies, although without clear significance for every stimulus tested (statistics as above). In response to the natural call, there were no strong differences between PAC_{FAF} and PAC_{AC} in the δ–θ/γ_{low} range, and effect sizes were also not large (Figure 5a). In the case of the 5.28 Hz (Figure 5b) and the Poisson (Figure 5c) syllabic trains, differences in the PAC across structures were stronger, reaching significance ($p_{corr} < .05$; grey contour lines) mostly at a depth of 450 μm for δ–θ/γ_{low} frequencies. Although for this frequency range significant differences between FAF and AC did not occur with PAC values calculated in response to the Poisson train (compare Figure 5b and Figure 5c, bottom rows depicting PAC differences for the 5.28 Hz and the Poisson stimuli), large effect sizes were still observed for δ–θ/γ_{low} frequencies (purple contour lines in Figure 5 marking areas where $PAC_{AC} > PAC_{FAF}$). Overall, these results indicate that the FAF and the AC engage in distinct phase-amplitude coupling dynamics comprising delta, theta, low- and high-gamma bands of the LFP.

3.4 | Quantitative changes of PAC across stimulus conditions

We compared the effect of different stimulus conditions on the z-scored PAC values (zMIs) in frontal and auditory cortices. To that end, we first evaluated differences between zMIs calculated during spontaneous activity and acoustic stimulation (Figure 6), and then differences of coupling values across different stimuli (Figure 7; see below). Considering the FAF, there were no significant differences between zMIs obtained during spontaneous activity compared to those related to acoustic stimulation (Figure 6a-c; FDR-corrected Wilcoxon signed rank tests, $p_{corr} > .05$). In the AC, however, stimulus-related zMIs were significantly lower ($p_{corr} < .05$; statistics as above) than zMIs quantified from spontaneous activity. This effect was consistent across stimuli at depths ≥ 450 μm from the cortical surface, although in the case of the natural call there was also significance in superficial electrodes (i.e. 50 μm; Figure 6a). Such differences in PAC profiles from the AC occurred mostly in the delta-theta/gamma range, wherein large effect sizes were observed (particularly in the case of stimulation with the natural call; purple contour lines in Figure 6). In the case of the other two acoustic streams (Figure 6b,c for the 5.28 Hz and the Poisson syllabic trains, respectively), differences were less pronounced, but still occurred at depths ≥ 450 μm and in the delta-theta/gamma frequency bands.

Stimulus-related changes of the coupling values obtained from both structures were examined by subtracting PAC profiles in response to different sounds (i.e. 5.28 Hz train vs. natural call, Poisson train vs. natural call, and Poisson train vs. 5.28 Hz train) within region. The differences resulting from these comparisons are illustrated in Figure 7. Stimulation with the natural sequence and the 5.28 Hz syllabic train elicited quantitatively similar PAC patterns in FAF and AC, resulting in no significant differences between these two stimuli (except very small areas in Figure 7a; FDR-corrected Wilcoxon signed rank tests,

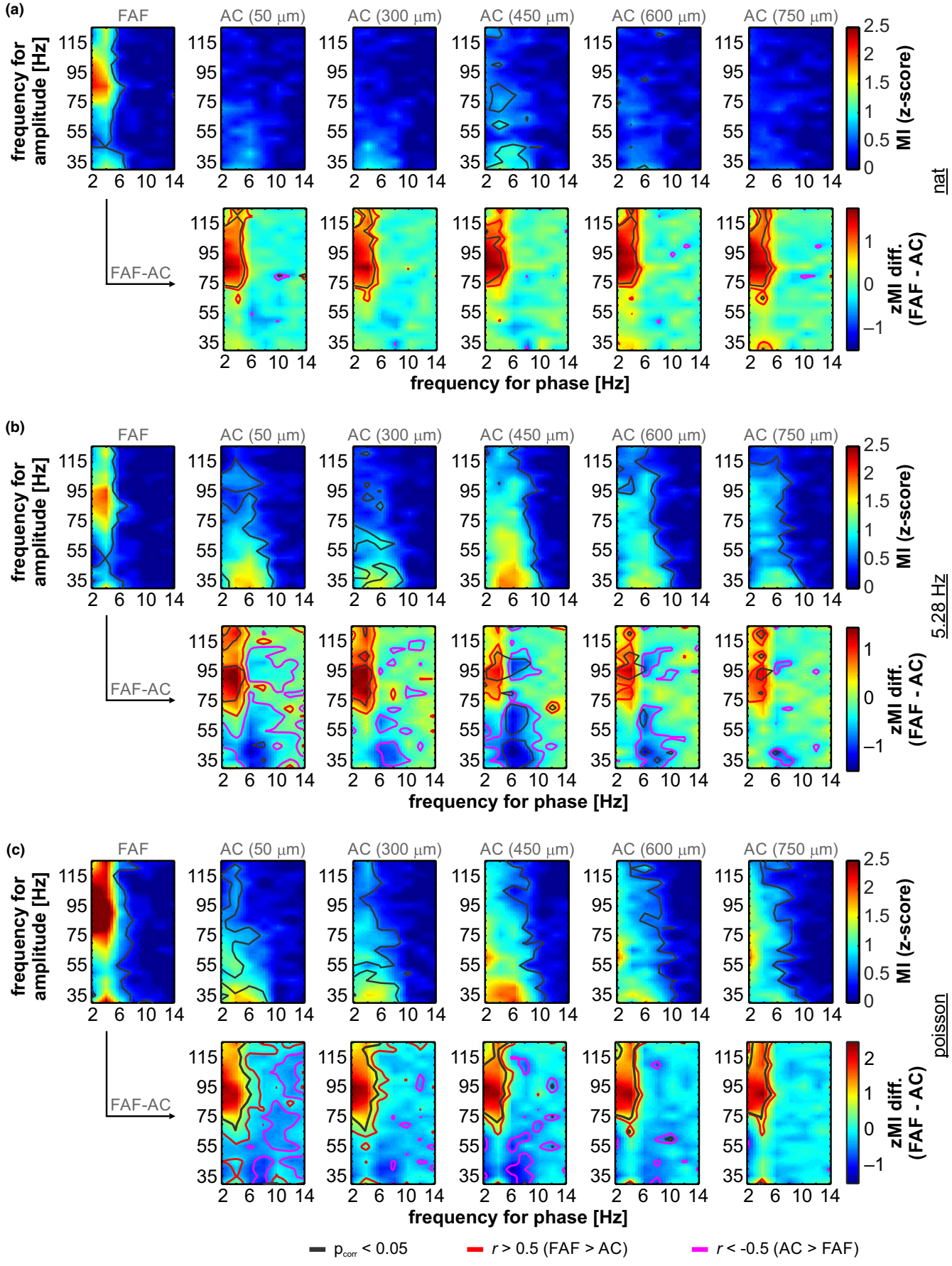
(a)
FAF
AC (50 μm)
AC (300 μm)
AC (450 μm)
AC (600 μm)
AC (750 μm)
frequency for amplitude [Hz]
115
95
75
55
35
2 6 10 14
2.5
2
1.5
1
0.5
0
MI (z-score)
nat
FAF-AC
1
0
−1
zMI diff. (FAF - AC)
frequency for phase [Hz]
(b)
5.28 Hz
(c)
poisson
p_corr < 0.05
r > 0.5 (FAF > AC)
r < -0.5 (AC > FAF)

FIGURE 5 PAC in FAF and AC during acoustic stimulation. (a) (*Top row*) Population-averaged PAC maps calculated from LFPs recorded in the FAF and the AC at various depths (50, 300, 450, 600, 750 µm), in response to the natural call used as stimulus in this study. Grey contour lines delimit regions where the z-normalized MI was significantly higher than 0 across penetrations ($n = 50$; FDR-corrected Wilcoxon signed rank test, $p_{corr} < .05$). (*Bottom row*) Population-averaged difference maps between FAF and AC (PAC_{FAF} - PAC_{AC}, at various depths in the AC: 50, 300, 450, 600, 750 µm; $n = 50$, same as above). Red contour lines delimit regions where $PAC_{FAF} > PAC_{AC}$, with large effect sizes ($r > 0.5$), whereas purple contour lines demarcate regions where the opposite occurred (i.e. $PAC_{AC} > PAC_{FAF}$), also with large effect sizes. Grey contour lines mark regions wherein the z-normalized MIs in FAF and AC were significantly different, according to a FDR-corrected Wilcoxon signed rank test, with an alpha of 0.05. (b-c) Same as in A, but LFPs were recorded in response to the 5.28 Hz (b) and the Poisson (c) syllabic trains

significance when $p_{corr} < .05$). However, stimulating with the Poisson sequence did significantly affect the values of PAC when compared to zMIs obtained with the other two sounds. PAC values related to the Poisson syllabic train were stronger in FAF than coupling values related to the natural call at δ/γ_{high} frequencies (Figure 7b; same statistics as above, grey contour lines indicate regions of significant differences; purple contour lines indicate regions of large effect size, $r < -0.5$). In the AC, there were significant differences occurring mostly at depths of 750 µm, with frequencies of 1-4/55-100 Hz (phase/amplitude signals). The gamma frequencies in which the PAC profiles were different were lower than the high-gamma frequency coupled to delta oscillations in FAF (75–120 Hz). This suggests that significant differences in the AC at 750 µm between the Poisson and the natural stimuli are mostly driven by the average syllable repetition rate in the Poisson train (70 Hz). When considering differences between the PAC related to the Poisson and 5.28 Hz trains (Figure 7c), the PAC related to the former was significantly stronger than the PAC related to the latter in FAF, once more for δ/γ_{high} frequencies ($p_{corr} < .05$, with large effect

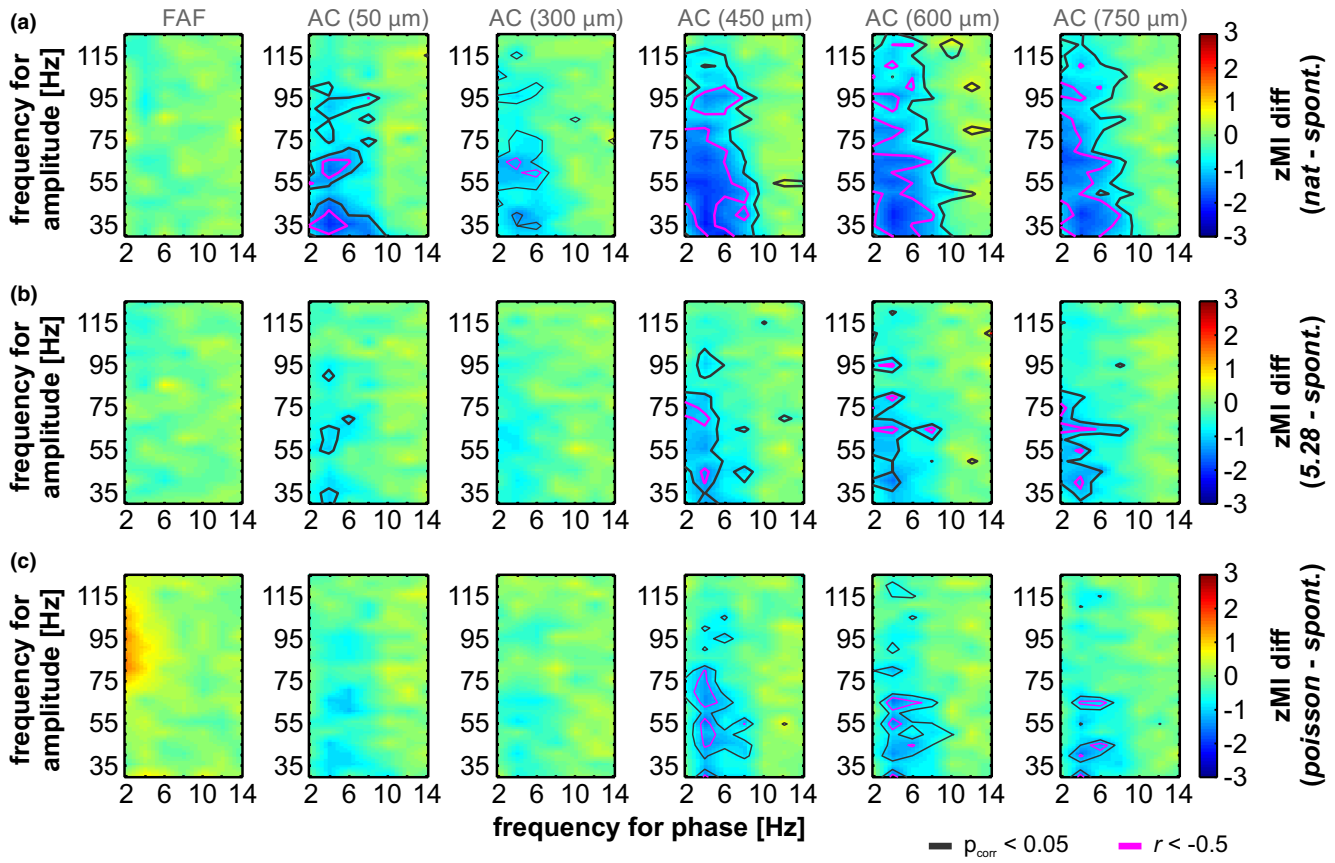

FIGURE 6 PAC differences across spontaneous and sound driven activities. (a) Population-averaged difference maps in the FAF and the AC (the latter structure at depths of 50, 300, 450, 600, 750 µm; $n = 49$), considering z-scored PAC values obtained from LFPs recorded during spontaneous activity and stimulation with the natural call. Blue colours in the figure indicate stronger zMIs during spontaneous activity in comparison to the zMIs related to acoustic stimulation; red colours indicate the opposite. Grey contour lines delimit regions of statistical significance (FDR-corrected Wilcoxon signed rank tests, $p_{corr} < .05$). Magenta contour lines mark regions in the PAC profiles where the above differences occurred with large effect size ($r < -0.5$). (b) Data were shown as in A, but the stimulus considered was the 5.28 Hz syllabic train. (c) Data were shown as in A, except the acoustic stimulus was the Poisson syllabic train

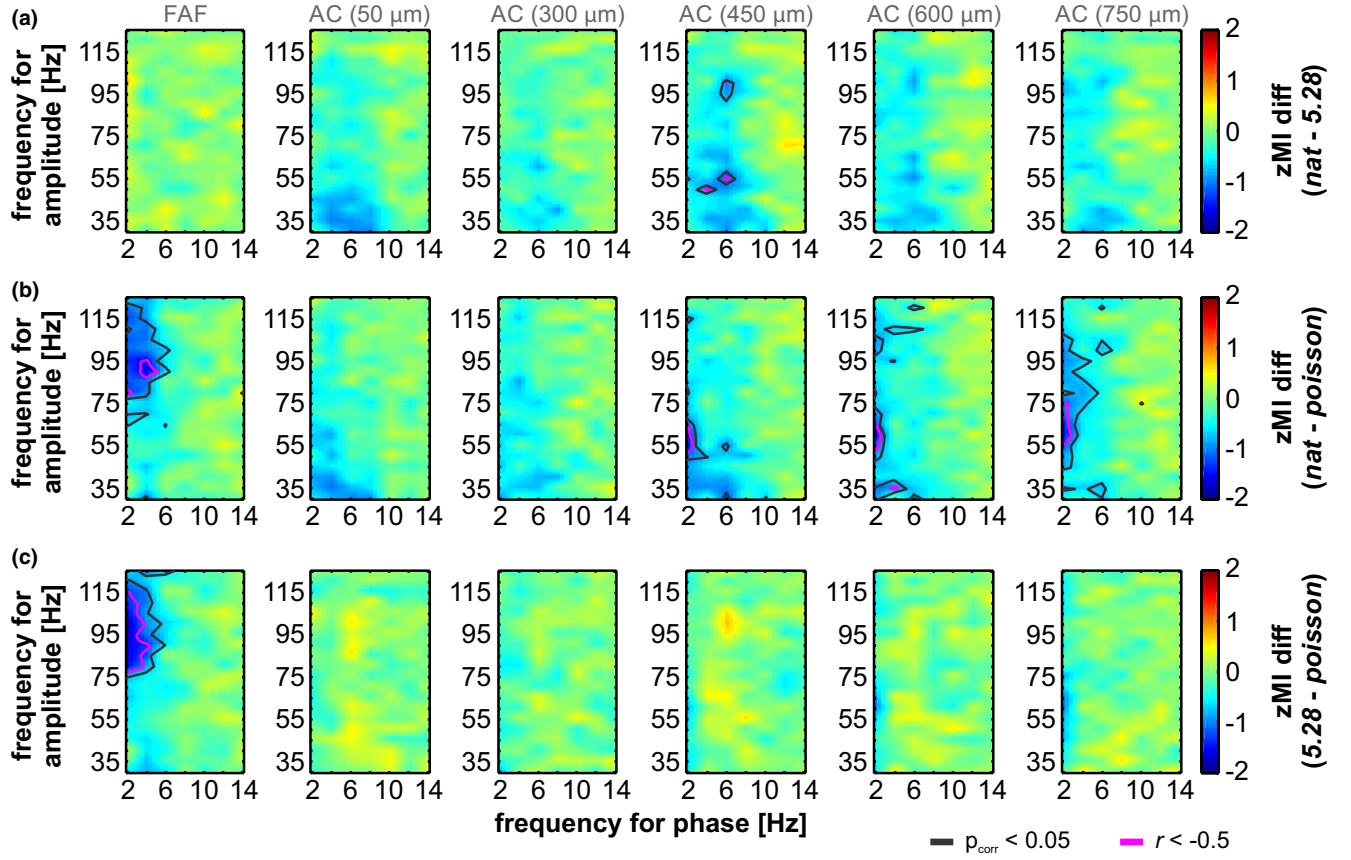

FIGURE 7 Differences in PAC across different acoustic stimuli. (a) Population-averaged difference maps in the FAF and the AC (the latter structure at depths of 50, 300, 450, 600, 750 µm; $n = 50$), taking into account the PAC obtained from LFPs recorded in response to the natural call and the 5.28 Hz syllable train. Red colours in the figure indicate stronger PAC during the natural call in comparison to the PAC during the 5.28 Hz train; blue colours indicate the opposite. Grey contours lines delimit regions in the PAC profile for which the coupling was significantly different between one stimulus and the other (FDR-corrected Wilcoxon signed-rank tests, $p_{corr} < .05$). Magenta lines mark areas in the profiles where the PAC differences occurred with large effect sizes ($r < -0.5$; i.e. the PAC related to the 5.28 Hz train was stronger than for the natural call). (b) Same as in A, comparing PAC values related to the natural call and the Poisson train stimuli. Red colours indicate stronger PAC during the natural call whereas blue colours indicate the opposite. Grey contour lines delimit areas in the PAC map of significant differences ($p_{corr} < .05$). Magenta contour lines indicate areas in the PAC map where the differences occurred with large effect size ($r < -0.5$; PAC during Poisson stimulation was stronger than during the stimulation with the natural call). (c) Same as in A and B, but comparing PAC values related to the 5.28 Hz and the Poisson syllabic trains. Red colours indicate stronger PAC during the 5.28 Hz train stimulation, whereas blue colours indicate the opposite. Grey contour lines delimit regions of significant differences in the map ($p_{corr} < .05$). Magenta contour lines demarcate areas in the PAC map where differences occurred with large effect size ($r < -0.5$; i.e. PAC related to the Poisson stimulus stronger than the PAC related to the 5.28 Hz train stimulus)

sizes; see Figure 7c). In contrast, we observed no significant differences in the AC. The data shown in Figure 7b, c indicates that the Poisson syllabic train stimulus alters zMI values in the FAF when compared to zMIs obtained from responses to the other stimuli, albeit with a less strong effect in the AC.

3.5 | Inter-areal PAC

Inter-areal PAC has been described as a mechanism for long-range neuronal interactions in sensory cortices, hippocampus and frontal regions of the brain (Bonnefond et al., 2017). To determine to what extent the FAF-AC network benefits from inter-areal PAC dynamics, we explored nested oscillatory coupling in the circuit when one structure provided the phase signal, and the other the amplitude signal. Here, analyses were the same as the ones used to estimate PAC within a single structure (i.e. AC or FAF), but mixing phase and amplitude recorded in different areas of the brain. Figures 8 and 9 depict the results obtained with this approach, first when the phase signal was provided by the FAF and the amplitude signal by the AC (Figure 8), and when the phase signal was obtained from the AC and the amplitude signal from the FAF (Figure 9). A diagram at the left of each figure represents the origins of phase-amplitude information. In our dataset, there was weak inter-areal PAC coupling, regardless of whether the phase information originated from electrodes in FAF or AC

(Figures 8 and 9, respectively; stimulus conditions are organized in rows: first, spontaneous activity; second, natural call; third, 5.28 Hz syllabic train; fourth, Poisson syllabic train). In fact, zMI values were not significantly above 0 at a population level, as results from statistical analyses did not survive corrections for multiple comparisons (FDR corrected, tailed Wilcoxon signed rank tests; significance when $p_{corr} < .05$). A trend of stronger PAC values obtained from delta-theta and gamma frequencies is observable (red colours in the figures; the trend is even clearer when calculating PAC with the Method from (Tort et al., 2010), shown in Figure S2), but such pattern is not enough evidence to assert cross-frequency interactions between FAF and AC at a network level when animals listen passively to acoustic stimuli.

4 | DISCUSSION

This study addressed the phase-amplitude coupling of oscillatory activities in the AC and FAF of the bat *C. perspicillata*. We report significant PAC in both structures during spontaneous activity and acoustic processing. However, the coupling between low- and high-frequency LFPs differed in auditory and frontal regions of the brain: in the AC, the PAC was strongest in the delta-theta/low-gamma range, while in the FAF the PAC peak occurred predominantly in delta/high-gamma frequencies. Thus, we show that *C. perspicillata's* AC and FAF exhibit distinct phase-amplitude coupling profiles.

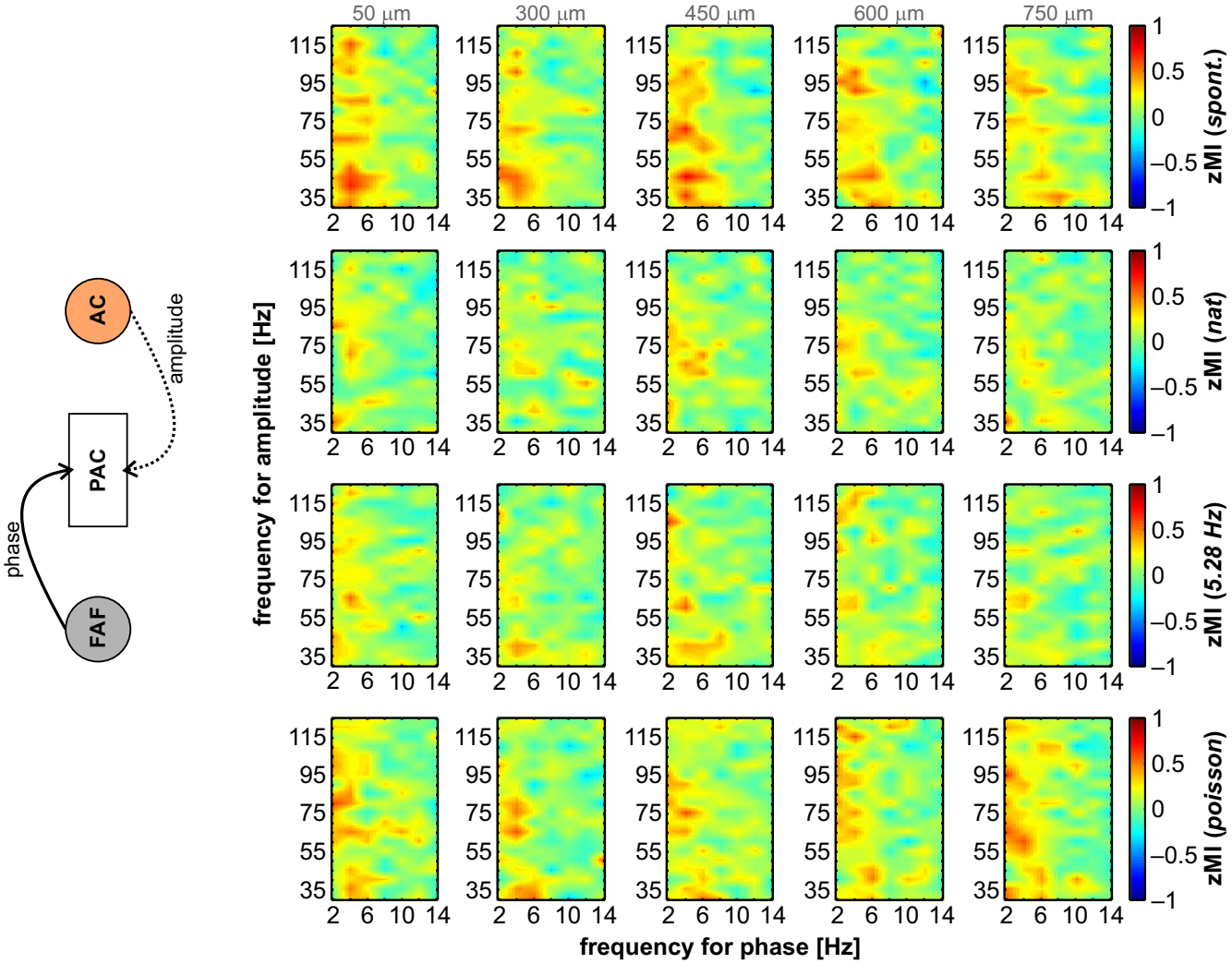

FIGURE 8 Inter-areal PAC: FAF phase and AC amplitude. The schematic on the left illustrates that for the PAC data shown in the figure LFPs recorded from the FAF provided the phase information, while LFPs recorded in the AC provided the amplitude information. On the right, each row shows the population-averaged PAC profiles ($n = 48$ during spontaneous activity, $n = 50$ during acoustic stimulation) obtained with the interareal analysis according the stimulation protocol. That is (from top to bottom): first row, inter-areal PAC during spontaneous activity; second row, inter-areal PAC during stimulation with the natural call; third row, inter-areal PAC when the stimulus was the 5.28 Hz syllabic train; fourth row, inter-areal PAC when the stimulus was the Poisson syllabic train

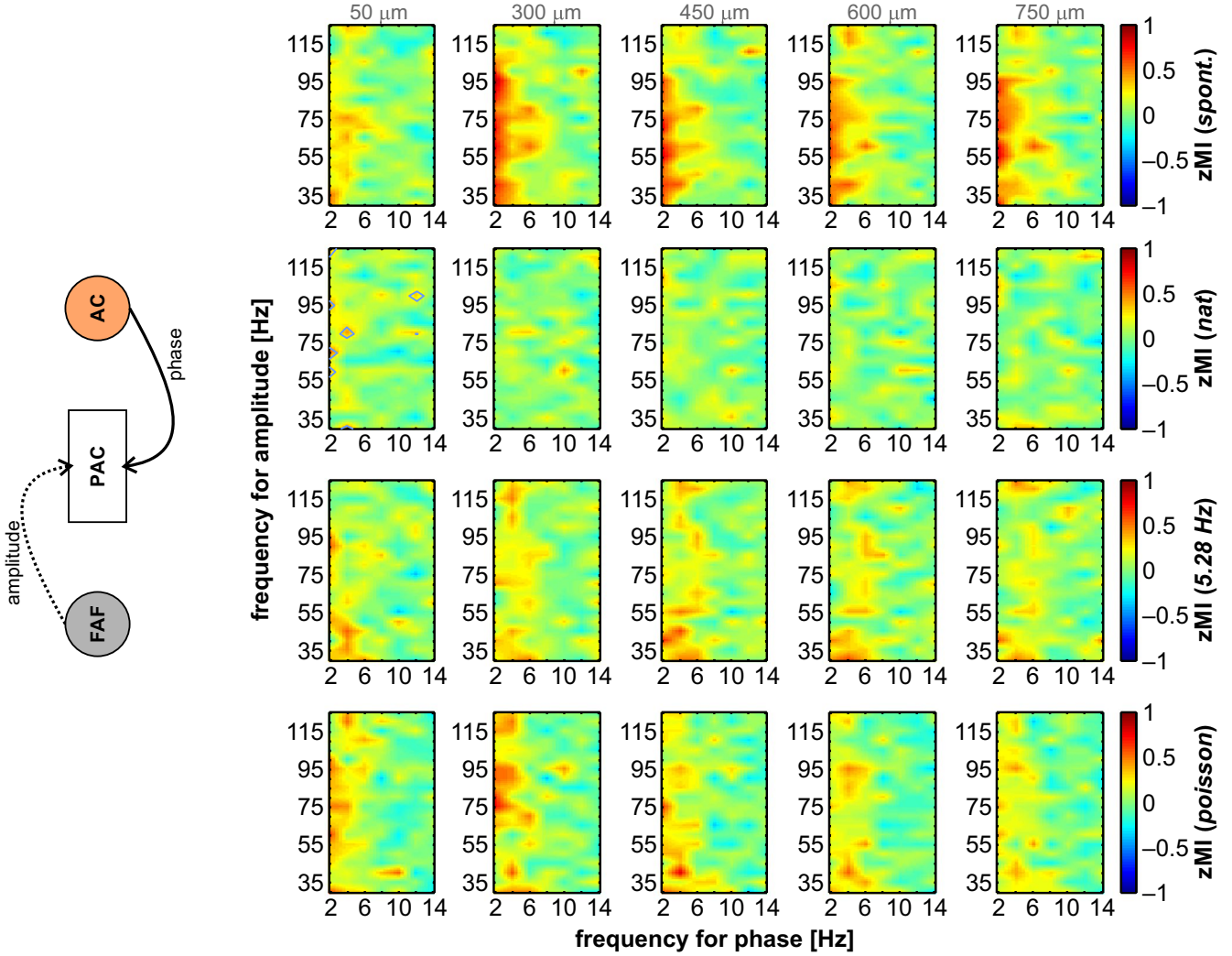

FIGURE 9 Inter-areal PAC: AC phase and FAF amplitude. This figure follows the conventions of Figure 8. The schematic on the left illustrates that, in this case, for PAC calculations LFPs from the FAF provided the amplitude information, whereas LFPs from the AC provided the phase information. On the right, each row depicts population-averaged inter-areal PAC profiles according to the stimulation protocol (from top to bottom: spontaneous activity, natural call stimulation, 5.28 Hz syllabic train stimulation, and Poisson syllabic train stimulation). There were $n = 48$ penetrations considered during spontaneous activity, and $n = 50$ penetrations considered during acoustic stimulation

4.1 | Phase-amplitude coupling in auditory and frontal areas

Phase-amplitude coupling could be important for the integration of distinct spatiotemporal dynamics represented via low- and high-frequency oscillations (Canolty & Knight, 2010; Hyafil, et al., 2015). Thus, the modulation of high-frequency amplitude by low-frequency phase constitutes a plausible and powerful mechanism of sensory processing, especially when the low frequency oscillations are influenced by external stimulation. A large body of evidence indicates that slow oscillatory activity in sensory cortices entrains (i.e. synchronizes) to the temporal structure of external stimuli (Brookshire et al., 2017; Doelling et al., 2019; García-Rosales, et al., 2018; Molinaro & Lizarazu, 2018; Sieben et al., 2013). Synchronized oscillatory activity can act as a sensory filtering mechanism (otherwise called "sensory selectivity") that is in turn susceptible to top-down modulation by processes such as attention (Calderone et al., 2014; Lakatos et al., 2008; Obleser & Kayser, 2019; Schroeder & Lakatos, 2009). Low frequency activity, coupled with gamma-band oscillations, could therefore align enhanced processing periods (marked by the gamma rhythms) to the structure of internal states or external inputs, thereby boosting their representation in the brain. Research in the human auditory cortex, for example, shows that theta-gamma PAC plays a major role for the efficient processing of speech signals (Gross et al., 2013; Lizarazu et al., 2019; Zion Golumbic et al., 2013). Indeed, computational modelling demonstrates that the

low-frequency stimulus-related neural oscillations might provide a temporal reference frame in which syllables can be processed by high-frequency activity coupled to the underlying slow rhythm (Hyafil, et al., 2015).

It is worth noticing that the effects of PAC in the auditory cortex generalize beyond speech processing. The coupling of low- and high-frequency oscillations could underpin the segmentation of continuous stimuli into behaviourally relevant "perceptual" units. Remarkably, the formation of perceptual auditory units could be important for echolocating bats such as *C. perspicilllata*. A bat exploring its surroundings using sonar receives a stream of incoming echoes corresponding to self-emitted echolocation pulses that reflect from external objects. The integration of those echoes at the level of the auditory or frontal cortices may allow the bat to form an acoustic picture of the environment. Such integration may find its mechanistic substrate in PAC interactions between oscillations working at slow, integrative timescales (e.g. delta, theta or alpha) and faster ones (e.g. gamma) that would encode the fine structure of the echo streams. Considering that *C. perspicillata* produces echolocation calls with a rate of 40–50 Hz (Beetz et al., 2019), and that LFPs in this bat's AC strongly synchronize to fast acoustic inputs also in the gamma range (Garcia-Rosales et al., 2019; Hechavarria et al., 2016b), the above-discussed possibility constitutes an interesting view that still requires empirical validation.

In general, it is plausible that PAC dynamics in sensory systems could complement the well-described roles of low-frequency activity for high-order sensory processing (Arnal et al., 2015). Hence, comparable PAC-related phenomena may occur not only across primate species, but also in other mammals. Considering that in the AC of *C. perspicillata* the neuronal representation of acoustic stimuli shares coding mechanisms similar to those described in the primate auditory and visual domains (Belitski et al., 2008, 2010; García-Rosales, et al., 2018; García-Rosales, et al., 2018; Kayser et al., 2009), the theta-gamma PAC reported in this study could also reflect a general mechanism shared across species. The spontaneous cross-frequency coupling in *C. perspicillata's* AC and FAF (Figure 4) further suggests that the relationship between slow and fast oscillations echoes the properties of cortical networks that do not directly depend on sensory inputs, but that can nevertheless be affected or modulated by them. We therefore propose that auditory cortical delta-theta/low-gamma coupling might provide in bats the same functional advantages proposed for other animals. These circuit dynamics might be evolutionarily preserved, being similar in phylogenetically distant species such as bats and primates.

The frontal cortex is considered an association area where sensory stimuli are integrated, and behavioural/cognitive functions are controlled (Carlen, 2017; Hage & Nieder, 2015; Hardung et al., 2017; Miller, 2000; Sugihara et al., 2006). These processes may be supported by oscillatory activity in frontal regions, which further allows coordination with distant areas in the brain including sensory systems and the hippocampus (Daume et al., 2017; Helfrich & Knight, 2016; Park et al., 2015). The frontal-auditory field, located in the bat frontal cortex (Eiermann & Esser, 2000; Kobler et al., 1987), receives auditory inputs from the AC and via a non-lemniscal pathway directly from the suprageniculate nucleus of the thalamus, bypassing major centres such as the inferior colliculus and the AC itself (Casseday et al., 1989; Kobler et al., 1987). The FAF is thus in a privileged position to integrate relatively "raw" auditory information arriving from the thalamus and arguably more processed inputs from the AC. It is likely that the response properties of the FAF, potentially explained by slow afferent synaptic dynamics (Lopez-Jury et al., 2019), constitute evidence for auditory integration in the frontal cortex. This integration can capitalize on PAC, combining low frequency oscillations, which could relate to integratory timescales, with high frequency activity, in turn marking local computations. Although the roles of the FAF for auditory-guided behaviour are not wholly clear, there is evidence indicating that oscillations in this region could coordinate inter-areal communication with the AC (García-Rosales et al., 2020), behavioural control either by motor commands or volitional vocalization production (Eiermann & Esser, 2000; Kobler et al., 1987; Weineck et al., 2020), and brain-to-brain synchronization during social interactions (Zhang & Yartsev, 2019).

Phase-amplitude coupling in FAF and AC occurs mostly at two distinct frequency regimes during spontaneous activity and sound processing (Figures 4-5). We speculate that the different δ/γ_{high} and δ–θ/γ_{low} coupling in frontal and auditory cortices, respectively, indicate that the properties and interactions between the neural substrates at the core of low- and high-frequency oscillations differ across structures. In the FAF-AC network, a possible way of integrating the activity of those substrates with different coupling (and oscillatory) dynamics would be by means of inter-areal PAC. The former need also be complemented by inter-regional phase coherence in the low frequency range (see (Bonnefond et al., 2017; Colgin et al., 2009; Helfrich & Knight, 2016; Hyafil, et al., 2015)), which we have shown in previous work to occur in *C. perspicillata* between frontal and auditory cortices, with and without acoustic stimulation (García-Rosales et al., 2020). In our dataset, however, we observe little evidence of active phase-amplitude coupling across regions (see Figures 8, 9, and Figure S2b). Rather, the reported inter-areal PAC patterns appear to be a vestige of two co-occurring phenomena: first, low-frequency LFP coherence in the FAF-AC circuit; and second, cross-frequency coupling between low- and high-frequencies within each structure. Although the inter-regional coupling (even if a consequence of the above-mentioned phenomena) might be sufficient to support network dynamics based on PAC, evidence from the current

dataset does not allow to assert consequential cross-frequency interactions between frontal and auditory cortices. It remains open to explore whether more complex experimental settings, wherein animals are required to do more than passively listen to acoustic stimulation, are necessary to drive robust inter-regional PAC with measurable functional implications. Further research in this direction is required to fully elucidate whether PAC supports the functional relationship between auditory and frontal cortices, bringing together local computations occurring at non-overlapping temporal scales in different gamma sub-bands, according to the synaptic properties of each region.

4.2 | Stimulation effects and respiratory rhythms: methodological considerations

From the data shown in Figure 6 it appears that z-scored PAC values during acoustic stimulation are lower than during spontaneous activity in the auditory cortex. These results, however, should be considered with care. Although the surrogate analyses for PAC calculation used with spontaneous data are similar in principle to those used with data related to acoustic stimulation, there are important differences that must be taken into account. zMIs associated to stimulus processing are ultimately determined by the surrogate methodology (i.e. the subtraction of the mean trial response from individual trials, and the across-trial randomization of phase and amplitude time series). Particularly in the AC, the LFP activity during sound processing is driven by the temporal structure of the acoustic input, which is most typically manifested through entrainment (i.e. phase-locking) of low- and high-frequency LFPs to the sound's temporal regularities (see (García-Rosales, et al., 2018; Garcia-Rosales et al., 2019)). There is thus an expected across-trial consistency of LFPs in the presence of stimulation that does not happen when randomly segmenting continuous LFP signals and treating each segment as a single trial, as done for the spontaneous activity. Tackling and minimizing the effects of such stimulus-dependent consistency, not present in the spontaneous data, were the main goals of the surrogate analyses implemented in this study. Therefore, lower zMIs during acoustic stimulation strongly suggest that stimulus-related PAC values are explainable to a high degree by robust across-trial consistent LFP activities, driven by the temporal structure of the acoustic inputs.

Acoustic stimulation with different sounds affects quantitatively (albeit not qualitatively) the PAC patterns in frontal and auditory cortices (Figure 7). Stimulation with the Poisson train, in particular, rendered significantly higher coupling values (mostly in FAF) than those observed when the stimuli were the natural sequence or the 5.28 Hz syllabic train. Although syllables are presented in the Poisson train non-periodically, the fact that they are repeated with an average rate of 70 Hz could have as a consequence an increase in gamma power in auditory regions, potentially leading to higher zMIs. We aimed at reducing stimulus-locked effects by implementing stringent surrogate procedures on the data (see above, and Methods), although direct modulations in the LFP from the external inputs cannot be entirely ruled out. Nonetheless, we note that the different PAC dynamics in frontal and auditory cortices reported in this study are not contingent on acoustic stimulation, as they occurred when sounds carried low and high frequency periodicities simultaneously (the natural call), or only low/high frequency rhythms (the 5.28 Hz and Poisson trains, respectively). Indeed, different PAC dynamics between FAF and AC were also observed without the presence of acoustic input (spontaneous activity; Figure 4).

The measurements of phase-amplitude coupling from neuronal oscillations can also be affected, beyond methodological caveats, by various physiological variables (Aru et al., 2015). For example, Tort and colleagues argue that respiratory rhythms, coupled with gamma-band activity, might influence PAC measurements in many cortical areas (Tort et al., 2018). It is nevertheless contended that respiration-related PAC and oscillatory activity are not necessarily artifactual, but that they may reflect cognitive processes and mechanisms for active sensing (Corcoran et al., 2018; Tort et al., 2018). In the particular case of the frontal cortex (where the FAF is located), respiration-related low-frequency oscillations (in the delta-theta bands) modulate a sub-band of gamma with frequencies ranging from 70–120 Hz (Zhong et al., 2017). Interestingly, this falls within the δ/γ_{high} range of this study (note Figures 4 and 5), which makes it possible that the PAC here reported carries signatures of respiration-gamma coupling. As we do not have data from respiratory rhythms recorded simultaneously with the neural activity, the extent of the possible modulation of PAC values by respiration in the FAF cannot be quantified. We note, however, that if respiration-coupled gamma activity in frontal areas subserve high-order perception (Corcoran et al., 2018; Tort et al., 2018), the PAC associated to respiration may also be important for sensory integration, particularly in the auditory and olfactory modalities. *C. perspicillata* bats rely on multimodal clues for navigation in naturalistic environments, for which olfaction and audition appear crucial (Thies et al., 1998). The interesting possibility of multimodal integration in FAF supported by oscillatory dynamics like PAC, and the extent to which it is modulated by endogenous oscillations that may or may not be related to respiratory rhythms, need to be thoroughly addressed in future experimental work.

ACKNOWLEDGEMENTS

The German Research Council (DFG) funded this work (Grant No. HE 7478/1-1, to JCH). Open access funding enabled and organized by ProjektDEAL.

CONFLICT OF INTERESTS

The authors declare no financial or non-financial conflict of interests.

AUTHOR CONTRIBUTION

FGR and JCH designed the study. FGR collected the data, analysed the data, and wrote the manuscript. FGR, LLJ, EGP, YCC, MK, and JCH discussed the results and reviewed the manuscript.

DATA AVAILABILITY STATEMENT

The data that support the findings of this study are available from the corresponding authors upon reasonable request.

PEER REVIEW

The peer review history for this article is available at https://publons.com/publon/10.1111/ejn.14986.

ORCID

Francisco García-Rosales https://orcid.org/0000-0001-5576-2967
Luciana López-Jury https://orcid.org/0000-0002-9384-2586
Julio C. Hechavarria https://orcid.org/0000-0001-9277-2339

REFERENCES

Amemiya, S., & Redish, A. D. (2018). Hippocampal theta-gamma coupling reflects state-dependent information processing in decision making. *Cell Reports*, *25*, 3894–3897. https://doi.org/10.1016/j.celrep.2018.12.057

Arnal, L. H., Flinker, A., Kleinschmidt, A., Giraud, A. L., & Poeppel, D. (2015). Human screams occupy a privileged niche in the communication soundscape. *Current Biology*, *25*, 2051–2056. https://doi.org/10.1016/j.cub.2015.06.043

Aru, J., Aru, J., Priesemann, V., Wibral, M., Lana, L., Pipa, G., Singer, W., & Vicente, R. (2015). Untangling cross-frequency coupling in neuroscience. *Current Opinion in Neurobiology*, *31*, 51–61. https://doi.org/10.1016/j.conb.2014.08.002

Axmacher, N., Henseler, M. M., Jensen, O., Weinreich, I., Elger, C. E., & Fell, J. (2010). Cross-frequency coupling supports multi-item working memory in the human hippocampus. *Proceedings of the National Academy of Sciences*, *107*, 3228–3233. https://doi.org/10.1073/pnas.0911531107

Beetz, M. J., Kossl, M., & Hechavarria, J. C. (2019). Adaptations in the call emission pattern of frugivorous bats when orienting under challenging conditions. *Journal of Comparative Physiology A*, *205*, 457–467. https://doi.org/10.1007/s00359-019-01337-1

Belitski, A., Gretton, A., Magri, C., Murayama, Y., Montemurro, M. A., Logothetis, N. K., & Panzeri, S. (2008). Low-frequency local field potentials and spikes in primary visual cortex convey independent visual information. *Journal of Neuroscience*, *28*, 5696–5709. https://doi.org/10.1523/JNEUROSCI.0009-08.2008

Belitski, A., Panzeri, S., Magri, C., Logothetis, N. K., & Kayser, C. (2010). Sensory information in local field potentials and spikes from visual and auditory cortices: Time scales and frequency bands. *Journal of Computational Neuroscience*, *29*, 533–545. https://doi.org/10.1007/s10827-010-0230-y

Benchenane, K., Peyrache, A., Khamassi, M., Tierney, P. L., Gioanni, Y., Battaglia, F. P., & Wiener, S. I. (2010). Coherent theta oscillations and reorganization of spike timing in the hippocampal- prefrontal network upon learning. *Neuron*, *66*, 921–936. https://doi.org/10.1016/j.neuron.2010.05.013

Bonnefond, M., Kastner, S., & Jensen, O. (2017). Communication between brain areas based on nested oscillations. *Eneuro*, *4*(2), ENEURO.0153-16.2017. https://doi.org/10.1523/ENEURO.0153-16.2017

Bosman, C. A., Schoffelen, J. M., Brunet, N., Oostenveld, R., Bastos, A. M., Womelsdorf, T., Rubehn, B., Stieglitz, T., De Weerd, P., & Fries, P. (2012). Attentional stimulus selection through selective synchronization between monkey visual areas. *Neuron*, *75*, 875–888. https://doi.org/10.1016/j.neuron.2012.06.037

Brookshire, G., Lu, J., Nusbaum, H. C., Goldin-Meadow, S., & Casasanto, D. (2017). Visual cortex entrains to sign language. *Proc Natl Acad Sci U S A*, *114*, 6352–6357. https://doi.org/10.1073/pnas.1620350114

Calderone, D. J., Lakatos, P., Butler, P. D., & Castellanos, F. X. (2014). Entrainment of neural oscillations as a modifiable substrate of attention. *Trends in Cognitive Sciences*, *18*, 300–309. https://doi.org/10.1016/j.tics.2014.02.005

Canolty, R. T., & Knight, R. T. (2010). The functional role of cross-frequency coupling. *Trends in Cognitive Sciences*, *14*, 506–515. https://doi.org/10.1016/j.tics.2010.09.001

Carlen, M. (2017). What constitutes the prefrontal cortex? *Science*, *358*, 478–482. https://doi.org/10.1126/science.aan8868

Casseday, J. H., Kobler, J. B., Isbey, S. F., & Covey, E. (1989). Central acoustic tract in an echolocating bat: An extralemniscal auditory pathway to the thalamus. *The Journal of Comparative Neurology*, *287*, 247–259. https://doi.org/10.1002/cne.902870208

Cho, R. Y., Konecky, R. O., & Carter, C. S. (2006). Impairments in frontal cortical gamma synchrony and cognitive control in schizophrenia. *Proceedings of the National Academy of Sciences of the USA*, *103*, 19878–19883.

Colgin, L. L., Denninger, T., Fyhn, M., Hafting, T., Bonnevie, T., Jensen, O., Moser, M. B., & Moser, E. I. (2009). Frequency of gamma oscillations routes flow of information in the hippocampus. *Nature*, *462*, 353–357. https://doi.org/10.1038/nature08573

Corcoran, A. W., Pezzulo, G., & Hohwy, J. (2018). Commentary: Respiration-entrained brain rhythms are global but often overlooked. *Frontiers in Systems Neuroscience*, *12*, 25. https://doi.org/10.3389/fnsys.2018.00025

Daume, J., Gruber, T., Engel, A. K., & Friese, U. (2017). Phase-amplitude coupling and long-range phase synchronization reveal frontotemporal interactions during visual working memory. *Journal of Neuroscience*, *37*, 313–322. https://doi.org/10.1523/JNEUROSCI.2130-16.2016

Doelling, K. B., Assaneo, M. F., Bevilacqua, D., Pesaran, B., & Poeppel, D. (2019). An oscillator model better predicts cortical entrainment to music. *Proceedings of the National Academy of Sciences USA*, *116*, 10113–10121. https://doi.org/10.1073/pnas.1816414116

Eiermann, A., & Esser, K. H. (2000). Auditory responses from the frontal cortex in the short-tailed fruit bat Carollia perspicillata. *NeuroReport*, *11*, 421–425.

Esghaei, M., Daliri, M. R., & Treue, S. (2015). Attention decreases phase-amplitude coupling, enhancing stimulus discriminability in cortical area MT. *Frontiers in Neural Circuits*, *9*, 82.

Esser, K. H., & Eiermann, A. (1999). Tonotopic organization and parcellation of auditory cortex in the FM-bat Carollia perspicillata. *European Journal of Neuroscience*, *11*, 3669–3682.

Fries, P. (2015). Rhythms for cognition: Communication through Coherence. *Neuron*, *88*, 220–235.

Fritz, C. O., Morris, P. E., & Richler, J. J. (2012). Effect size estimates: Current use, calculations, and interpretation. *Journal of Experimental Psychology: General*, *141*, 2–18.

García-Rosales, F., Beetz, M. J., Cabral-Calderin, Y., Kössl, M., & Hechavarria, J. C. (2018a). Neuronal coding of multiscale temporal features in communication sequences within the bat auditory cortex. *Communications Biology*, *1*, 200.

García-Rosales, F., López-Jury, L., González-Palomares, E., Cabral-Calderín, Y., & Hechavarría, J. C. (2020). Fronto-temporal coupling dynamics during spontaneous activity and auditory processing in the Bat Carollia perspicillata. *Frontiers in Systems Neuroscience*, *14*, 1–23.

García-Rosales, F., Martin, L. M., Beetz, M. J., Cabral-Calderin, Y., Kossl, M., & Hechavarria, J. C. (2018b) Low-frequency spike-field coherence is a fingerprint of periodicity coding in the auditory cortex. *iScience*, *9*, 47–62.

Garcia-Rosales, F., Rohrig, D., Weineck, K., Rohm, M., Lin, Y. H., Cabral-Calderin, Y., Kossl, M., & Hechavarria, J. C. (2019). Laminar specificity of oscillatory coherence in the auditory cortex. *Brain Struct Funct*, *224*, 2907–2924.

Giraud, A. L., & Poeppel, D. (2012). Cortical oscillations and speech processing: Emerging computational principles and operations. *Nature Neuroscience*, *15*, 511–517.

Gross, J., Hoogenboom, N., Thut, G., Schyns, P., Panzeri, S., Belin, P., & Garrod, S. (2013). Speech rhythms and multiplexed oscillatory sensory coding in the human brain. *PLoS Biology*, *11*, e1001752.

Hage, S. R., & Nieder, A. (2015). Audio-vocal interaction in single neurons of the monkey ventrolateral prefrontal cortex. *Journal of Neuroscience*, *35*, 7030–7040.

Hardung, S., Epple, R., Jackel, Z., Eriksson, D., Uran, C., Senn, V., Gibor, L., Yizhar, O., & Diester, I. (2017). A functional gradient in the rodent prefrontal cortex supports behavioral inhibition. *Current Biology*, *27*, 549–555.

Hechavarria, J. C., Beetz, M. J., Macias, S., & Kossl, M. (2016a). Distress vocalization sequences broadcasted by bats carry redundant information. *Journal of Comparative Physiology. A, Neuroethology, Sensory, Neural, and Behavioral Physiology*, *202*, 503–515.

Hechavarria, J. C., Beetz, M. J., Macias, S., & Kossl, M. (2016b). Vocal sequences suppress spiking in the bat auditory cortex while evoking concomitant steady-state local field potentials. *Scientific Reports*, *6*, 39226.

Helfrich, R. F., & Knight, R. T. (2016). Oscillatory dynamics of prefrontal cognitive control. *Trends in Cognitive Sciences*, *20*, 916–930.

Hyafil, A., Fontolan, L., Kabdebon, C., Gutkin, B., & Giraud, A. L. (2015). Speech encoding by coupled cortical theta and gamma oscillations. *Elife*, *4*, e06213.

Hyafil, A., Giraud, A. L., Fontolan, L., & Gutkin, B. (2015). Neural cross-frequency coupling: Connecting architectures, mechanisms, and functions. *Trends in Neurosciences*, *38*, 725–740.

Kayser, C., Montemurro, M. A., Logothetis, N. K., & Panzeri, S. (2009). Spike-phase coding boosts and stabilizes information carried by spatial and temporal spike patterns. *Neuron*, *61*, 597–608.

Kikuchi, Y., Attaheri, A., Wilson, B., Rhone, A. E., Nourski, K. V., Gander, P. E., Kovach, C. K., Kawasaki, H., Griffiths, T. D., Howard, M. A. 3rd, & Petkov, C. I. (2017). Sequence learning modulates neural responses and oscillatory coupling in human and monkey auditory cortex. *PLoS Biology*, *15*, e2000219.

Kobler, J. B., Isbey, S. F., & Casseday, J. H. (1987). Auditory pathways to the frontal cortex of the mustache bat, Pteronotus parnellii. *Science*, *236*, 824–826. https://doi.org/10.1126/science.2437655

Lakatos, P., Karmos, G., Mehta, A. D., Ulbert, I., & Schroeder, C. E. (2008). Entrainment of neuronal oscillations as a mechanism of attentional selection. *Science*, *320*, 110–113. https://doi.org/10.1126/science.1154735

Lakatos, P., Musacchia, G., O'Connel, M. N., Falchier, A. Y., Javitt, D. C., & Schroeder, C. E. (2013). The spectrotemporal filter mechanism of auditory selective attention. *Neuron*, *77*, 750–761. https://doi.org/10.1016/j.neuron.2012.11.034

Lisman, J. E., & Jensen, O. (2013). The theta-gamma neural code. *Neuron*, *77*, 1002–1016. https://doi.org/10.1016/j.neuron.2013.03.007

Lizarazu, M., Lallier, M., & Molinaro, N. (2019). Phase-amplitude coupling between theta and gamma oscillations adapts to speech rate. *Annals of the New York Academy of Sciences*, *1453*, 140–152. https://doi.org/10.1111/nyas.14099

Lopez-Jury, L., Mannel, A., Garcia-Rosales, F., & Hechavarria, J. C. (2019). Modified synaptic dynamics predict neural activity patterns in an auditory field within the frontal cortex. *European Journal of Neuroscience*, *51*(4), 1011–1025. https://doi.org/10.1111/ejn.14600

Magazzini, L., & Singh, K. D. (2018). Spatial attention modulates visual gamma oscillations across the human ventral stream. *NeuroImage*, *166*, 219–229. https://doi.org/10.1016/j.neuroimage.2017.10.069

Medalla, M., & Barbas, H. (2014). Specialized prefrontal "auditory fields": Organization of primate prefrontal-temporal pathways. *Front Neurosci*, *8*, 77.

Miller, E. K. (2000). The prefrontal cortex and cognitive control. *Nature Reviews Neuroscience*, *1*, 59–65.

Molinaro, N., & Lizarazu, M. (2018). Delta(but not theta)-band cortical entrainment involves speech-specific processing. *European Journal of Neuroscience*, *48*, 2642–2650.

Morillon, B., Liegeois-Chauvel, C., Arnal, L. H., Benar, C. G., & Giraud, A. L. (2012). Asymmetric function of theta and gamma activity in syllable processing: An intra-cortical study. *Front Psychol*, *3*, 248. https://doi.org/10.3389/fpsyg.2012.00248

Obleser, J., & Kayser, C. (2019). Neural entrainment and attentional selection in the listening brain. *Trends in Cognitive Sciences*, *23*, 913–926. https://doi.org/10.1016/j.tics.2019.08.004

O'Connell, M. N., Barczak, A., Ross, D., McGinnis, T., Schroeder, C. E., & Lakatos, P. (2015). Multi-scale entrainment of coupled neuronal oscillations in primary auditory cortex. *Frontiers in Human Neuroscience*, *9*, 655. https://doi.org/10.3389/fnhum.2015.00655

Park, H., Ince, R. A., Schyns, P. G., Thut, G., & Gross, J. (2015). Frontal top-down signals increase coupling of auditory low-frequency oscillations to continuous speech in human listeners. *Current Biology*, *25*, 1649–1653. https://doi.org/10.1016/j.cub.2015.04.049

Plakke, B., & Romanski, L. M. (2014). Auditory connections and functions of prefrontal cortex. *Front Neurosci-Switz*, *8*. https://doi.org/10.3389/fnins.2014.00199

Schroeder, C. E., & Lakatos, P. (2009). Low-frequency neuronal oscillations as instruments of sensory selection. *Trends in Neurosciences*, *32*, 9–18. https://doi.org/10.1016/j.tins.2008.09.012

Sieben, K., Roder, B., & Hanganu-Opatz, I. L. (2013). Oscillatory entrainment of primary somatosensory cortex encodes visual control of tactile processing. *Journal of Neuroscience*, *33*, 5736–5749. https://doi.org/10.1523/JNEUROSCI.4432-12.2013

Sotero, R. C., Bortel, A., Naaman, S., Mocanu, V. M., Kropf, P., Villeneuve, M. Y., & Shmuel, A. (2015). Laminar distribution of phase-amplitude coupling of spontaneous current sources and sinks. *Frontiers in Neuroscience*, *9*, 454. https://doi.org/10.3389/fnins.2015.00454

Spaak, E., Bonnefond, M., Maier, A., Leopold, D. A., & Jensen, O. (2012). Layer-specific entrainment of gamma-band neural activity by the alpha rhythm in monkey visual cortex. *Current Biology*, *22*, 2313–2318. https://doi.org/10.1016/j.cub.2012.10.020

Sugihara, T., Diltz, M. D., Averbeck, B. B., & Romanski, L. M. (2006). Integration of auditory and visual communication information in the primate ventrolateral prefrontal cortex. *Journal of Neuroscience*, *26*, 11138–11147. https://doi.org/10.1523/JNEUROSCI.3550-06.2006

Thies, W., Kalko, E. K. V., & Schnitzler, H. U. (1998). The roles of echolocation and olfaction in two Neotropical fruit-eating bats, Carollia perspicillata and C-castanea, feeding on Piper. *Behavioral Ecology and Sociobiology*, *42*, 397–409. https://doi.org/10.1007/s002650050454

Tort, A. B. L., Brankack, J., & Draguhn, A. (2018). Respiration-entrained brain rhythms are global but often overlooked. *Trends in Neurosciences*, *41*, 186–197. https://doi.org/10.1016/j.tins.2018.01.007

Tort, A. B., Komorowski, R., Eichenbaum, H., & Kopell, N. (2010). Measuring phase-amplitude coupling between neuronal oscillations of different frequencies. *Journal of Neurophysiology*, *104*, 1195–1210. https://doi.org/10.1152/jn.00106.2010

Tort, A. B., Komorowski, R. W., Manns, J. R., Kopell, N. J., & Eichenbaum, H. (2009). Theta-gamma coupling increases during the learning of item-context associations. *Proceedings of the National Academy of Sciences USA*, *106*, 20942–20947. https://doi.org/10.1073/pnas.0911331106

van Driel, J., Cox, R., & Cohen, M. X. (2015). Phase-clustering bias in phase-amplitude cross-frequency coupling and its removal. *Journal of Neuroscience Methods*, *254*, 60–72. https://doi.org/10.1016/j.jneumeth.2015.07.014

Wang, D., Clouter, A., Chen, Q., Shapiro, K. L., & Hanslmayr, S. (2018). Single-trial phase entrainment of theta oscillations in sensory regions predicts human associative memory performance. *Journal of Neuroscience*, *38*, 6299–6309. https://doi.org/10.1523/JNEUROSCI.0349-18.2018

Weineck, K., Garcia-Rosales, F., & Hechavarria, J. C. (2020). Neural oscillations in the fronto-striatal network predict vocal output in bats. *PLoS Biology*, *18*, e3000658. https://doi.org/10.1371/journal.pbio.3000658

Xiao, Z., Martinez, E., Kulkarni, P. M., Zhang, Q., Hou, Q., Rosenberg, D., Talay, R., Shalot, L., Zhou, H., Wang, J., & Chen, Z. S. (2019). Cortical pain processing in the rat anterior cingulate cortex and primary somatosensory cortex. *Frontiers in Cellular Neuroscience*, *13*, 165. https://doi.org/10.3389/fncel.2019.00165

Zhang, W., & Yartsev, M. M. (2019). Correlated neural activity across the brains of socially interacting bats. *Cell*, *178*(413–428), e422. https://doi.org/10.1016/j.cell.2019.05.023

Zhong, W., Ciatipis, M., Wolfenstetter, T., Jessberger, J., Muller, C., Ponsel, S., Yanovsky, Y., Brankack, J., Tort, A. B. L., & Draguhn, A. (2017). Selective entrainment of gamma subbands by different slow network oscillations. *Proceedings of the National Academy of Sciences USA*, *114*, 4519–4524. https://doi.org/10.1073/pnas.1617249114

Zion Golumbic, E. M., Ding, N., Bickel, S., Lakatos, P., Schevon, C. A., McKhann, G. M., Goodman, R. R., Emerson, R., Mehta, A. D., Simon, J. Z., Poeppel, D., & Schroeder, C. E. (2013). Mechanisms underlying selective neuronal tracking of attended speech at a "cocktail party". *Neuron*, *77*, 980–991. https://doi.org/10.1016/j.neuron.2012.12.037

SUPPORTING INFORMATION

Additional supporting information may be found online in the Supporting Information section.

How to cite this article: García-Rosales F, López-Jury L, González-Palomares E, Cabral-Calderín Y, Kössl M, Hechavarria JC. Phase-amplitude coupling profiles differ in frontal and auditory cortices of bats. *Eur J Neurosci* 2020;00:1–19. https://doi.org/10.1111/ejn.14986